1

Introduction to Gallium Nitride Properties and Applications

Fabrizio Roccaforte[1] *and Mike Leszczynski*[2,3]

[1] *Consiglio Nazionale delle Ricerche – Istituto per la Microelettronica e Microsistemi (CNR-IMM), Strada VIII, n. 5 – Zona Industriale, 95121 Catania, Italy*
[2] *Institute of High Pressure Physics – Polish Academy of Sciences (Unipress-PAS), Sokolowska 29/37, 01-142 Warsaw, Poland*
[3] *TopGaN Sp. z o.o., Sokolowska 29/37, 01-142 Warsaw, Poland*

1.1 Historical Background

Since some decades, gallium nitride (GaN) and other related materials (e.g. ternary AlGaN and InGaN and quaternary InAlGaN) have been used for optoelectronic components. Moreover, some of these nitrides are also recently emerging as promising semiconductors for the next generation of power electronic devices. In fact, the introduction of GaN-based materials in power electronics can enable a better efficiency of the devices and a reduction of the electric power consumption. Hence, the overall nitride device market forecasts for the next years are much brighter compared to those of the other compound semiconductors.

For those reasons, the revolution expected in modern electronics and optoelectronics is often regarded, half-jokingly, as "*GaNification*."

This book gives an overview on the main nitride semiconductor technologies for power electronic and optoelectronic devices: transistors, diodes, light-emitting diodes (LEDs), laser diodes (LDs), etc. The way to these devices has been long and not easy because nitrides are very difficult to be grown and processed. The present chapter is an introduction to properties and applications of GaN and related materials.

The history of GaNification can be dated back to the early 1930s and since then it has been characterized by many important milestones, leading to the creation of the key technologies for electronic and optoelectronic devices. A summary of important historical steps of nitrides research is reported below:

- 1932: The first polycrystalline GaN material was synthesized by flowing ammonia (NH_3) over liquid gallium (Ga) at elevated temperatures [1]. This material was examined, proving its stability up to 800 °C in hydrogen atmosphere.
- 1938: The crystal structure of GaN has been studied on GaN powders [2].

Nitride Semiconductor Technology: Power Electronics and Optoelectronic Devices,
First Edition. Edited by Fabrizio Roccaforte and Mike Leszczynski.

- 1969–1971: Thin GaN layers were grown by Maruska and Tietjen [3] using hydride vapor-phase epitaxy (HVPE) on sapphire substrates. Because of a large lattice mismatch of these two materials, the layers exhibited a poor crystallographic quality. However, this material was used for confirming the direct energy band gap (3.39 eV) and for demonstrating the first LED concepts [4].
- 1972: Manasevit et al. [5, 6] grew the first metal–organic vapor-phase epitaxy (MOVPE) GaN layers. This method became the most popular one in nitride technology, and today, there are a few thousands of reactors worldwide. However, these layers were still rough and not transparent (they looked like frosted glass) because of the lattice mismatch between sapphire and GaN.
- 1984: The thermodynamics studies by Karpinski et al. [7, 8] enabled the authors to find the way of growing bulk GaN crystals from the nitrogen solution in gallium (HPSG – high-pressure solution growth). However, the growth conditions necessary to avoid GaN decomposition were extreme: about 1200 °C and 10 kbar. This work clarified the unfeasibility to grow GaN crystals from the melt (i.e. Czochralski or Bridgman methods) because tens of kilobars have to be used to melt GaN at temperatures higher than 2500 °C.
- 1986: Hiroshi Amano from the group of Isamu Akasaki (Nagoya University) made a real breakthrough in GaN epitaxy by introducing a low-temperature AlN nucleation layer [9]. Such a nucleation layer enabled Amano and Akasaki to obtain smooth and transparent GaN with good crystallographic quality.
- 1989: Amano et al. [10] obtained for the first time p-type GaN by activating Mg dopants by low-energy electron irradiation. This activation was induced by breaking Mg—H bonds, inherently present in the MOVPE GaN layers (hydrogen is always incorporated together with Mg).
- 1990: Matsuoka et al. [11] succeeded in the growth of the first InGaN layers, offering an access to a very wide spectral range from 0.7 eV (IR) to 3.5 eV (UV), through all wavelengths of the visible range.
- 1991–1992: Shuji Nakamura (Nichia Chemical Corporation) optimized the growth conditions of GaN on sapphire using the AlN nucleation layer. This technology has been used by most of the companies and academic laboratories for fabricating LEDs and other devices. The dislocation density of such GaN on sapphire was in the order of 10^8–10^9 cm^{-2}. Moreover, annealing above 600 °C in nitrogen atmosphere led to the electrical activation of p-GaN layers [12, 13]. These studies paved the way to all LED and LD technologies.
- 1992: Nichia started offering blue LEDs (450 nm), which were used soon for illuminating phosphor to get white light. At present, such LEDs are being produced in millions every day, creating a multibillion market.
- 1993: Using MOVPE, Asif Khan et al. [14] grew the first AlGaN/GaN heterojunction. Despite a moderate crystallographic quality, the mobility of the two-dimensional electron gas (2DEG) at the AlGaN/GaN interface was around 600 $cm^2/V\,s$. This achievement can be regarded as a start of quest to nitride high electron mobility transistor (HEMTs) technology [15].
- 1996: The first violet LD (405 nm) based on InGaN quantum wells (QWs) was demonstrated by Nakamura et al. [16]. The laser was made on sapphire substrate, although it was clear that the use low defect density bulk GaN substrates

could lead to better performance. At that time, using the only available small HPSG bulk GaN crystals enabled Nakamura to increase the LD lifetime from 300 to 3000 hours.

- 1997: Bernardini et al. [17] determined the spontaneous and piezoelectric polarization constants of nitrides, improving the comprehension of the physics of AlGaN/GaN heterostructures and paving the way to the optimization of many electronic and optoelectronic devices.
- 1998: The first LEDs epi structures grown on silicon substrates by molecular beam epitaxy (MBE) were reported by Guha and Bojarczuk [18]. The MBE method provided some advantages over MOVPE, as the lack of hydrogen during growth, or the lower growth temperature. However, until now, most of the nitride technologies are based on MOVPE. The structures grown by Guha and Bojarczuk had a bad crystallographic quality but triggered research on epitaxy technology using silicon wafers as substrates.
- 1999: Ambacher et al. [19] proposed a model to analytically describe the 2DEG properties in AlGaN/GaN heterostructures. This model is today widely adopted by the GaN community. In the same year, Sheppard et al. [20] demonstrated high-power microwave HEMTs based on AlGaN/GaN heterostructures grown on the silicon carbide (SiC) substrate.
- 2000: The nature of the 2DEG was further clarified by Ibbetson et al. [21], attributing a key role to the surface states present in nitride materials as source of electrons.
- 2001: Sumitomo Electric bought patent from Tokyo Agriculture University on the DEEP method (dislocation elimination by the epitaxial-growth with inverse-pyramidal pits) [22, 23] to grow GaN single crystals on GaAs substrates using the HVPE method and bowing dislocations in small regions. This technology enabled Sumitomo to start fabricating bulk GaN substrates with low dislocation density (10^5 cm^{-2}) at the areas designated for laser stripes to make a commercial production of LDs by Nichia.
- 2003: Sony introduced Blu-ray DVD format based on 405 nm LDs fabricated by Nichia.
- 2006: Saito et al. [24] and Cai et al. [25] proposed, respectively, the recessed gate structure and fluorine implantation to achieve normally-off AlGaN/GaN HEMTs.
- 2007: Uemoto et al. [26] from Panasonic demonstrated the first normally-off HEMT based on the p-GaN gate technology. This device was also called gate injection transistor (GIT) as hole injection from a p-AlGaN layer resulted in an increase of the drain current because of the conductivity modulation. In 2009, EPC announced the commercialization of the first devices based on this technology.
- 2008: The first GaN-based vertical cavity surface emitting laser (VCSEL) operating at low temperature was demonstrated by Tien-Chang Lu and coworkers at the National Chiao Tung University (Hsinchu, Taiwan) [27].
- 2012: AlGaN/GaN heterostructures on 200 mm Si(111) substrates were demonstrated by Tripathy et al. [28]. The possibility to grow such heterostructures on large-area Si wafers opened the way to integrate

GaN HEMT device fabrication in Si CMOS (complementary metal–oxide semiconductor) fabs.

- 2013: Iveland et al. [29] provided experimental evidence that the "droop effect" (efficiency drop for high injection current in LEDs) is related to Auger electrons.
- 2013: High-frequency (HF) performances of GaN-based HEMTs, with ultra-high cutoff frequency f_t exceeding 450 GHz, were achieved through innovative device scaling technologies [30].
- 2014: The Noble Prize in Physics was assigned to three Japanese scientists (Isamu Akasaki, Hiroshi Amano, and Shuji Nakamura) for "*the invention of efficient blue light-emitting diodes which has enabled bright and energy-saving white light sources*"(www.nobelprize.org/prizes/physics/2014/summary).
- 2014: Recessed gate Al_2O_3/AlGaN/GaN normally-off MOS-HEMTs with reduced leakage current, high blocking voltage (825 V), and high threshold voltage (2.4 V) were demonstrated on 200 mm silicon substrates [31].
- 2015–2017: The first high-voltage (600 V) normally-off GaN HEMT solution, based on the "cascode" configuration, is released to the market by Transphorm [32]. Moreover, the progresses in the technology of p-GaN gate HEMTs resulted in the first fully industrial qualified "true" normally-off devices from Panasonic and Infineon [33–35].
- 2017: Haller et al. [36] gave a model for point defect formation at high growth temperature before the InGaN QWs, explaining their detrimental effect on LED efficiencies.
- 2017: LG Innotek introduced 100 mW UV-C LEDs into the market (www.powerelectronictips.com/worlds-first-100-mw-deep-uv-led).
- 2017: Mei et al. [37] demonstrated quantum dot VCSELs covering the "green gap."
- 2019: Zhang et al. [38] demonstrated 271.8 nm LD operating at room temperature and in the pulse mode.

1.2 Basic Properties of Nitrides

Nitride semiconductors (GaN, AlGaN, InAlN, InGaN, InAlGaN, AlN, etc.) possess a number of properties, which make them very useful for many optoelectronic and microelectronic applications. Table 1.1 reports the main physical properties of GaN and other nitrides in comparison with other semiconductors, highlighting some implications in material growth, optoelectronics, and power- and high-frequency electronics.

As can be seen, these materials exhibit several advantages for optoelectronic and power electronics, mainly related to their direct band gap, or the wide band gap (WBG) and high critical field. However, there are also a number of features, which make the material growth and the technology of devices very difficult. All these aspects will be discussed in more detail in the following sections, as well as in the other chapters of this book.

Table 1.1 Properties of GaN and other nitrides in comparison with other semiconductors and their implications in material growth, optoelectronics, and power- and high-frequency electronics [39–48].

	Property	Value/range	Comparison with other semiconductors
Material growth	Density, ρ	6.1 g/cm^3 (GaN)	Because of the high melting point and low decomposition temperature, nitride crystals (bulk and epi) are grown at low temperatures. Therefore, the crystals (substrates) cannot be grown from the melt as other semiconductors. Moreover, the epilayers grown at low temperatures have a large number of imperfections
	Atomic density	4.37×10^{22} atoms/cm^3 (GaN)	
	Melting point	2573 °C at 60 kbar for GaN, 1100 °C for InN, 2200 °C for AlN	
	Decomposition temperature at 1 bar	900 °C for GaN 600 °C for InN	
	Small influence of dislocations on luminosity of InGaN QWs and on electron scattering at low currents		Blue/green GaN-based LEDs and HEMTs can be fabricated using foreign substrates (Si, sapphire, and SiC)
	High critical Peierls–Nabarro shear stress for slip systems $\langle 11\bar{2}3\rangle\{11\bar{2}2\}$ and $\langle 11\bar{2}3\rangle\{1\bar{1}01\}$	29.8–54.7 GPa	Dislocations do not move upon stress or illumination (no degradation of optoelectronic devices related to dislocation motion as it is the case for other III–V materials)
Optoelectronics	Direct band gap	From 0.7 eV (InN) to 6.1 eV (AlN)	Nitrides dominate in the green/blue/UV spectral range. II–VI compounds are comparable, but they are too fragile to be used in devices. In infrared and red spectral range, GaAs- and InP-based devices have still much higher efficiencies

(Continued)

Table 1.1 (Continued)

	Property	Value/range	Comparison with other semiconductors
	Build-in internal electric field	Up to 2 MV/cm (InGaN/GaN)	The strong build-in internal electric field increases the spatial separation of electrons and holes, thus reducing the efficiency of radiative recombination in optoelectronic devices
Power/high-frequency (HF) electronics	Wide band gap, E_g	From 3.4 eV (GaN) to 6.1 eV (AlN)	Possible applications of GaN-based materials in high-voltage, high-power, and high-temperature electronics, in competition with SiC (and possibly in future, with Ga_2O_3 and diamond). The high defects density still hinders the full exploitation of the electric field strength
	Critical electric field, E_{CR}	3–3.75 MV/cm (GaN)	
	Electron affinity, χ	3.1–4.1 eV (GaN)	
	Dielectric constant, ε_r	9.5 (GaN)	
	Intrinsic carrier concentration, n_i	$\approx 10^{-10}$ cm^{-3} (GaN) at room temperature	Low leakage currents and high operation temperatures are possible, if the GaN material quality is improved
	Electron saturation velocity, v	3×10^7 cm/s (GaN)	Enable the fabrication of devices operating at high frequencies, in competition with the traditional GaAs technology
	Electron mobility, μ_n	1100–2000 cm^2/V s (GaN, AlGaN/GaN)	
	Thermal conductivity, κ	1.3–2.1 W/cm K (GaN)	Comparable to Si but significantly lower than SiC and diamond, making the heat dissipation a concern for GaN-based power devices

1.2.1 Microstructure and Related Issues

The specificity of nitride microstructure is dominated by three factors: (i) the main crystallographic form of GaN, AlN, and InN is the wurtzite, with high built-in electric fields; (ii) large lattice mismatches between substrates and epilayers, as well as between layers that form a device epi structure; and (iii) low growth temperatures.

The thermodynamically stable crystal phase of nitride semiconductors at room temperature and atmospheric pressure is the hexagonal wurtzite structure. For GaN, the wurtzite crystal structure is schematically depicted in Figure 1.1, where the unit cell, highlighted with bold lines, is characterized by the lattice parameters a_0 (3.189 Å) and c_0 (5.185 Å) [50, 51]. The Ga and N atoms are arranged in two interpenetrating hexagonal closely packed lattices, with a shift of 3/8 c_0.

In the hexagonal wurtzite structure, GaN has no inversion symmetry in the [0001] direction (the so-called *c*-axis). For that reason, it is possible to distinguish two different orientations of GaN crystals, i.e. the *Ga-face* (Figure 1.1a) and the *N-face* (Figure 1.1b), depending on whether the material is grown with Ga or N on top. These two faces have different chemical properties: Ga-face is more chemically inert and may behave differently during growth (e.g. the Ga-face incorporates easier acceptors, whereas the N-face incorporates easier donors [52]).

The covalent bonds allow each atom to be tetrahedrally bonded to four atoms of the other type. In addition, an ionic contribution is also present because of the large difference in electronegativity of Ga and N atoms. Because nitrogen has a higher electronegativity than gallium, Ga and N atoms will exhibit anionic and cationic characteristics, respectively, thus resulting in a *spontaneous polarization* $\boldsymbol{P}_{SP}$ oriented along the *c*-axis [53].

The spontaneous polarization exists even in the absence of strain. The strength of the spontaneous polarization depends on the asymmetry of the crystal. In fact, $\boldsymbol{P}_{SP}$ increases with decreasing the c_0/a_0 ratio. For example, a GaN crystal with a

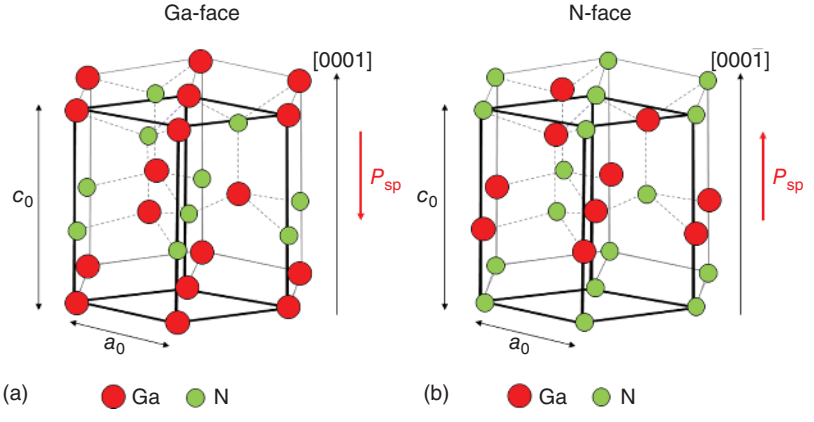

Figure 1.1 Hexagonal crystal structure of GaN (wurtzite) for the Ga-face (a) and for the N-face (b). The bold lines highlight the unit cell, while the dashed lines indicate the Ga—N bonds. The spontaneous polarization vectors ($\boldsymbol{P}_{SP}$) are also drawn for the two cases. Source: Reproduced with permission of Roccaforte et al. [49]. Copyright © 2018, Società Italiana di Fisica.

Table 1.2 Lattice parameters of AlN, GaN, and InN [50, 54–56].

Parameters	AlN	GaN	InN
a_0 (Å)	3.1113	3.1878	3.537
c_0 (Å)	4.9814	5.1850	5.703

c_0/a_0 ratio of 1.6259 has a lower P_{SP} (-0.029 C/m^2) with respect to an AlN crystal (-0.081 C/m^2) having a c_0/a_0 ratio of 1.6010 [17]. The negative values of the polarization indicate that the vector $\boldsymbol{P}_{SP}$ is pointing opposite to the [0001] direction, as illustrated in Figure 1.1 [17, 50]. It is worth mentioning that the external stress changing the ideality of the structure and the c_0/a_0 ratio can induce an additional contribution to the polarization called *piezoelectric polarization* $\boldsymbol{P}_{PE}$. This contribution is particularly important in AlGaN/GaN heterostructures for the generation of 2DEG, as will be discussed in Section 1.2.4.

For the fabrication of power electronic and optoelectronic devices (e.g. diodes, transistors, LEDs, and LDs), the suitable epitaxial structures must be grown on appropriate substrates. The lattice parameters are important for determining the suitability of a material as a substrate for GaN epitaxy. Table 1.2 reports the values of the lattice parameters of AlN, GaN, and InN.

Here, it must be pointed out that in the literature, it is possible to find different data for InN and AlN because of the material differences with respect to their defect concentration. In addition, many papers report the lattice parameters of nitrides together with the thermal expansion coefficients (TECs), which may lead to wrong conclusions, as the TECs vary with temperature [56–58].

Most of the research and technologies of nitrides are based on the epitaxy on foreign substrates [59] because GaN and AlN single crystals are still small and expensive.

Table 1.3 reports the lattice and thermal mismatch between GaN and the most popular foreign substrates: sapphire (Al_2O_3), silicon (Si), and silicon carbide (SiC). The typical ranges of the dislocation density measured in GaN layers grown on these substrates, the possible device layout (lateral or vertical), and application fields of the materials are also reported in the table.

Sapphire is a common substrate used for GaN heteroepitaxy for optoelectronic applications. However, GaN exhibits large lattice (+16%) and TEC mismatch (-34%) with respect to Al_2O_3 substrate, typically resulting into a high defect density of the grown GaN epilayers. Hence, a better choice is represented by the hexagonal silicon carbide (6H/4H–SiC) with a lattice mismatch of only 3.5%. The first GaN-based transistors for power switching applications were demonstrated on (0001) *c*-plane sapphire and (0001) silicon carbide (6H–SiC and 4H–SiC) [20, 39, 62]. However, in spite of the small lattice mismatch, a high dislocation density (10^7–10^8 cm^{-2}) is still present in GaN layers grown on SiC [63]. Moreover, the cost of SiC substrates has always represented a limiting factor for the introduction of this technology in consumer electronic products.

At the beginning of the last decade, great efforts have been devoted to the development of GaN on Si substrates [60]. In fact, Si offers low price in

Table 1.3 Lattice and thermal mismatch between GaN and the most popular foreign substrates (Al_2O_3, Si, and SiC).

Properties and applications of GaN layers on different substrate	GaN-on-Al_2O_3	GaN-on-SiC	GaN-on-Si	GaN-on-GaN
Lattice mismatch (%)	16	3.5	−17	0
Thermal expansion coefficient mismatch, a_0 (%)	−34	21.4	53.5	0
Dislocation density (cm^{-2})	10^7–10^8	10^7–10^8	10^8–10^9	10^3–10^6
Device layout	Lateral	Lateral	Lateral	Lateral and vertical
Main application areas	Optoelectronics	HF electronics, optoelectronics	HF and power electronics	HF and power electronics, optoelectronics

Relevant information for device applications of GaN epilayers (dislocation density, possible device type, and application fields) are also reported [43, 59–61].

comparison with sapphire and SiC, a high crystalline perfection, and the availability of large-size substrates. Clearly, the lattice mismatch between GaN(0001) with respect to Si(111) is very large (−17%), and consequently, a high dislocation density (in the order of 10^9 cm^{-2}) is generated in the material.

The difference in the TECs between GaN and its substrate also plays an important role in the epitaxial process and, hence, in the final quality of the active layer for the device. Sapphire has a higher TEC than GaN, leading to residual compressive stress in the grown GaN layer, while the TECs of SiC and Si are smaller, resulting in residual tension [64]. The value of the residual stresses depends on the growth conditions, as at the growth temperature, the GaN layers are not fully relaxed but can be strained because of grain coalescence [65].

To overcome the problem of residual strain, in the case of GaN-on-Si, several "strain management" techniques are adopted to mitigate crack formation in the GaN epitaxial layers (e.g. appropriate AlN or graded AlGaN buffer layers, AlN/GaN superlattices, or sophisticated lithographic patterning techniques of the substrates [39, 66]). In this context, the rapid progresses in epitaxial growth of GaN materials resulted in the demonstration of electronic grade large-area GaN-on-Si heterostructures up to 200 mm in diameter, and power devices with excellent efficiency and compact size have started to be implemented on these materials [28, 31, 66, 67].

Clearly, bulk GaN would be the ideal substrate for GaN epitaxy and device fabrication. In fact, a significant reduction of the dislocation density (down to 10^3–10^6 cm^{-2}) is possible using bulk GaN [61]. So far, such substrates are used for LD fabrication. Besides that, the possibility of fabricating vertical devices (not

possible when GaN is grown on foreign substrates) would represent a big advantage for power electronic applications. However, until now, several obstacles have hindered a widespread implementation of bulk GaN power devices, including the high cost and the limited diameter of commercially available substrates [61].

The lattice mismatch is a problem not only in heteroepitaxy but also in GaN homoepitaxy. In fact, it has been reported that free electrons expand the lattice of GaN [68]. For example, the free electrons of concentration 5×10^{19} cm^{-3} expand the lattice of GaN by about 0.3%. Although this lattice expansion may seem not significant, it can lead to serious problems in the growth of bulk GaN crystals, as different crystal faces incorporate different impurities (mainly oxygen) and contain different free electron concentrations.

In majority of cases, the growth of nitrides is in the $\langle 0001 \rangle$ direction. It is the most natural one for nitrides to get a good crystallographic quality. Moreover, p-type doping is more efficient when the growth is in this direction [69]. However, for other directions, the internal electric fields, separating electrons and holes in LEDs, are smaller. Therefore, there have been attempts to use GaN substrates or templates oriented along nonpolar directions of $\langle 10\bar{1}0 \rangle$ and semipolar ones of $\langle 11\bar{2}2 \rangle$ to increase the efficiency of optoelectronic devices. Despite the big research efforts done, the advantage of nonpolar or semipolar device epi structures has not been proven yet, and almost all commercial devices are constructed on polar wafers.

In epitaxy, the on-axis orientations are seldom used. In most of the cases, off-cut substrates are used to grow epi layers in step-flow growth mode [70]. The substrate off-cut influences the epilayers under different points of view, such as the point defects formation, the indium incorporation in InGaN layers, the lattice distortions, and surface roughness. For example, Suski et al. [71] showed a higher hole concentration for GaN:Mg grown on the off-cut Ga-face GaN substrate. Sarzyński et al. [72] observed a decrease of indium content for InGaN grown on the off-cut Ga-face GaN substrate. On the other hand, triclinic distortion of the strained epi layers was reported by Krysko et al. [73]. Also, the surface morphology is influenced by the off-cut angle, as a smaller roughness was observed in the GaN layer grown on the off-cut N-face GaN substrate [74].

All optoelectronic devices emitting in visible region are based on InGaN QWs, which are extremely difficult to be grown because of large lattice mismatch to GaN and of low growth temperatures. In this context, a widely discussed topic is the occurrence of indium spatial fluctuations in the QW [75–77]. These fluctuations may appear in the nanometer, micrometer, and even millimeter scale.

An example of indium fluctuations in InGaN/GaN QWs, visualized by high spatial resolution secondary ion mass spectrometry (SIMS), is shown in Figure 1.2. Their amplitude and dimensions strongly depend on growth conditions, dislocation density, and layer morphology (e.g. local terrace width) [72].

Concerning InGaN, special attention should be devoted to the influence of hydrogen on indium incorporation. In fact, even a small percentage of hydrogen significantly decreases the indium incorporation [78–80]. However, hydrogen smoothens the surfaces, so it can be used during the InGaN or GaN barrier growth. The smoother the surface is, the smaller the indium fluctuation should be.

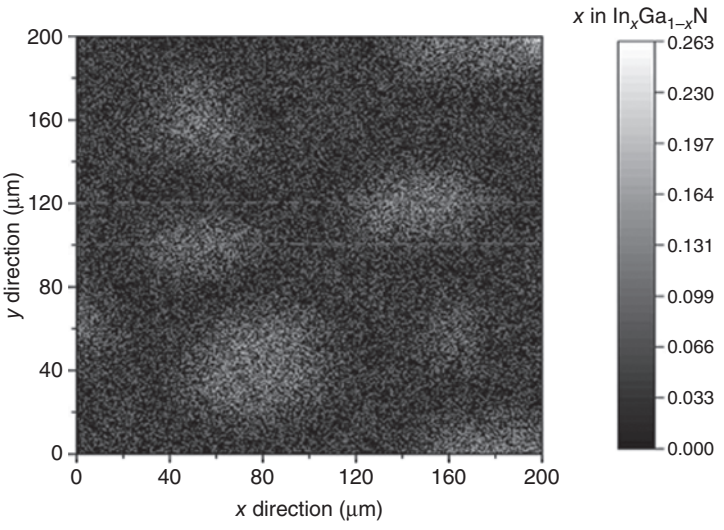

Figure 1.2 SIMS *x*–*y* image showing the lateral distribution of indium in a InGaN/GaN QW. The vertical scale indicates the In-concentration *x* in $In_xGa_{1-x}N$. Source: Adapted with permission of Michałowski et al. [77]. Copyright © 2019, Royal Society of Chemistry.

InGaN layers and QWs evolve when they are subjected to high temperatures; for example, when they are overgrown by p-type GaN:Mg. Although at low temperature the InGaN layers may get homogenized, an increase of the temperature (>900 °C) leads to InGaN decomposition. Both phenomena occur because of easy indium diffusion, most probably through Ga-vacancies. This topic will be discussed in Chapter 2.

When the InGaN layers exceed critical values of strain and thickness, they get relaxed by misfit dislocations [81]. An example of a net of misfit dislocations in InGaN is shown in Figure 1.3.

It is worth mentioning that the relaxation of the InGaN layers may be not only a plastic one (via emission of dislocations), but also an elastic one in three-dimensional nano-objects on the surface (poor morphology). Therefore, InGaN relaxation should be monitored not only using X-ray diffraction

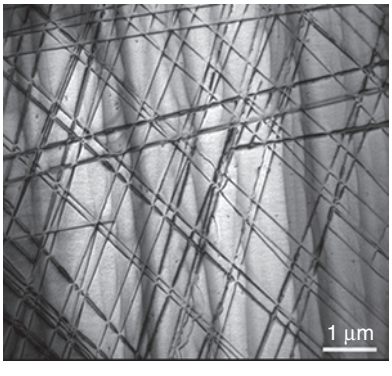

Figure 1.3 TEM plan view bright-field image with diffraction vector $\mathbf{g}_{11-20}$ of the MBE-grown 50 nm InGaN layer, with an In content of 20%. Source: Courtesy of Johanna Moneta.

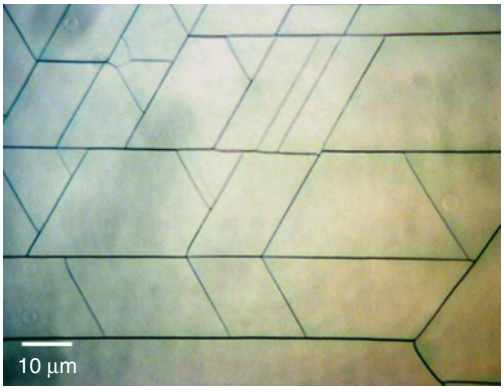

Figure 1.4 Optical microscopy view of a 220 nm thick $Al_{0.27}Ga_{0.73}N$ layer grown on a GaN substrate.

(XRD) but also using atomic force microscopy (AFM), transmission electron microscopy (TEM), and defect-selective etching (DES).

Nitride transistors for power- and high-frequency devices, as well as UV emitters, are based on AlGaN layers. The main microstructural problem encountered with the AlGaN layers is their tendency to be cracked because of the tensile strain when they are grown on GaN (e.g. in AlGaN/GaN heterostructures for transistors). Figure 1.4 shows, as an example, an optical microscopy image of a thick AlGaN layer grown on GaN, showing the presence of cracks on the surface.

In order to avoid cracking, lateral patterning [82] or compliance layers [83] are applied as technological solutions.

Cracks are obviously a serious concern in GaN heteroepitaxy on Si substrates, as they act as scattering centers that reduce the carrier mobility and, hence, the performance of the transistors. In this case, several methods have been reported to eliminate the cracks in AlGaN/GaN heterostructures grown on Si(111) substrates and to improve the crystal quality, such as the use of graded $Al_xGa_{1-x}N$ interlayers between an AlN buffer layer and GaN, or the introduction of AlGaN/GaN superlattices [84].

Although extended defects, as dislocations, can be easily detected and their density is measured using selective etching, XRD, or TEM, much more difficult is the detection of point defects. Ga-vacancies (acceptor-like defects) can be measured using positron annihilation, but only in the case of thick layers (not QWs). In the case of nitrogen vacancies, there is no direct method to detect them. Therefore, only theoretical models can be used to explain various properties of nitrides, such as diffusion of atoms, luminosity, or electrical properties, based on indirect assumptions of the presence of point defects.

In summary, nitride semiconductors for optoelectronics and power electronics have a complex microstructure, which is characterized by a large number of imperfections: dislocations, point defects, poor morphology, non-uniform strains, non-uniform electric fields, and non-uniform atom distribution. All these imperfections are not independent of each other and may influence the optical and electrical properties. Moreover, all those imperfections depend on the growth parameters (temperature, pressure, gases flows, reactor geometry, etc.). Hence, the complex microstructure, as well as the large number of growth

parameters, makes the optimization of the crystal quality a very challenging issue for GaN and related nitrides.

1.2.2 Optical Properties

Nitrides possess direct band gaps from 0.7 eV (InN), through 3.4 eV (GaN) to 6.1 eV (AlN). Hence, they cover the spectral range from infrared (1770 nm) through the visible range up to far ultraviolet (about 200 nm) [85]. Figure 1.5 reports the values of the energy gap for nitride semiconductors as a function of the in-plane lattice parameter.

For a ternary nitride compound $A_xB_{1-x}N$, the energy band gap does not change linearly with the composition x, but it follows a phenomenological expression:

$$E_g^{A_xB_{1-x}N}(x) = xE_g^A + (1-x)E_g^B - x(1-x)b \tag{1.1}$$

where b is bowing parameter (in units of eV), defined as the coefficient of the parabolic term. A positive value of b indicates a downward bowing, while a negative b indicates an upward bowing in the dependence of the energy gap E_g on the composition x.

Typically, in nitride compounds, most of the measurements of the energy gap (and hence of the bowing parameter) are performed using emission techniques, such as photoluminescence (PL) and cathodoluminescence (CL).

The most important materials for optoelectronics are QWs and wires of InGaN. The optical properties of these QWs have been reported in thousands of papers, but still they contain many unrevealed secrets. For InGaN, the reported values of the bowing parameter b range from 1.4 to 2.8 eV [86]. Such a large span is related to the variability of the InGaN properties (indium fluctuations, non-homogeneous QW thickness), already mentioned in Section 1.2.1. The compositional inhomogeneities of the alloy and even inherent hole localization in random alloys [87] lead to strong Stokes shift and underestimation of the band gap [88]. Moses and Van de Walle [89] suggested that the bowing parameter of InGaN is dependent on the composition.

On the other hand, AlGaN alloys are important for both optoelectronic and power- and high-frequency electronic devices. For AlGaN alloys, the values of

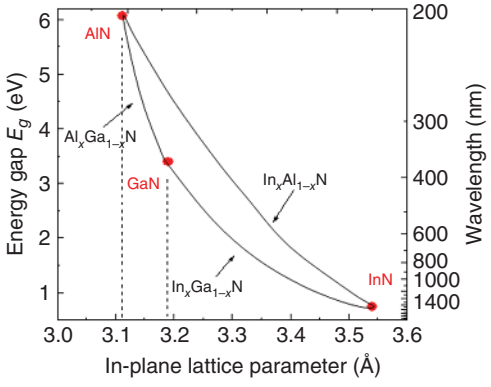

Figure 1.5 Energy band gap of nitride semiconductors (AlN, GaN, InN, and their ternary alloys) as a function on the in-plane lattice parameter. The corresponding wavelength is reported on the right axis.

the bowing parameter b reported in the literature vary from −0.8 to 2.6 eV, most likely emanating from AlGaN alloys prepared by different techniques with various qualities and, in some cases, a range of alloy compositions explored to be narrow. Yun et al. [90] reported a systematic study of the $Al_xGa_{1-x}N$ band gap as a function of the Al concentration x. By fitting the experimental data using Eq. (1.1), a bowing parameter $b = 1.0$ eV was obtained [90].

Optical transmission (OT) or optical absorption (OA) measurements provide a better estimation of the energy gap of nitrides. However, it is not easy to grow thick nitride layers (InGaN and AlGaN) necessary for such measurements. Moreover, OT and OA do not take into account energy dispersion of the refractive index, whose contribution to the band gap should not be neglected. The alternative measurement method that can meet the demands for the accurate energy band gap bowing is spectroscopic ellipsometry [91]. This method has been used for the estimation of the bowing parameter of nitrides and has the major advantage of determining the complex dielectric function of the investigated material.

In general, the PL and CL spectra measured on nitrides consist of excitonic part and defect-related part [92]. For example, for bulk GaN, the following spectral features are typically identified: (i) excitonic part: free excitons and bound excitons; (ii) donor–acceptor pairs (DAPs); and (iii) defect-related luminescence. An example of a PL spectrum for GaN is shown in Figure 1.6.

As mentioned already, even the simplest compound of GaN possess a large variety of point and extended defects, which affect the position, full width at half maximum (FWHM), and intensity of the PL peaks. A good review of optical properties of GaN was given by Reschikov and Morkoç [93].

In the case of ternary or quaternary compounds, the situation is much more complicated than for GaN, as one may deal with chemical composition fluctuations. The main information from the PL or CL peak is its wavelength position. For InGaN QWs, it depends on several factors: average indium content, indium fluctuations, QW thickness (for thin QWs, there is quantum effect of the

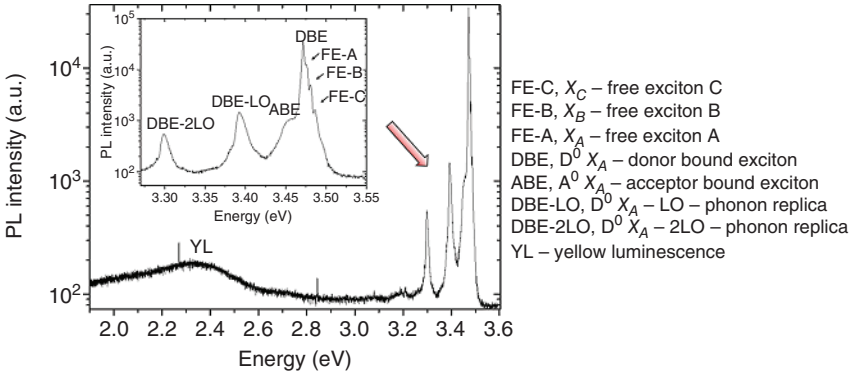

Figure 1.6 Typical photoluminescence (PL) spectrum for a GaN layer grown on sapphire substrate. Besides the excitonic part of the spectrum, a broad peak is present in the yellow region (about 550 nm), which can be related to point defects (Ga-vacancies and carbon impurity). Source: Courtesy of Grzegorz Staszczak.

blue shift, and for thick QWs, there is a separation of electrons and holes by the electric field resulting in the red shift), QW thickness variations, and presence of point defects. The position of the PL or CL peaks also depends on excitation power, which makes the analysis of the data extremely cumbersome. However, even more troublesome is the analysis of PL/CL peak intensity. In fact, besides the factors mentioned above, the peak intensity also depends on the absorption around the QWs and the diffusion length of minority carriers.

Additional information can be obtained by using time-resolved photoluminescence (TRPL) or time-resolved cathodoluminescence (TRCL). The decay times of the luminescence peaks can be interpreted by radiative and non-radiative recombination of electrons and holes. The experimental luminescence decay time (τ) is related to the radiative (τ_r) and non-radiative (τ_{nr}) decay times:

$$\frac{1}{\tau} = \frac{1}{\tau_r} + \frac{1}{\tau_{\mathrm{nr}}} \tag{1.2}$$

For binary compounds, long decay times can be observed for the nearly perfect crystals. For the particular case of InGaN QWs, the long decay times can also be attributed to indium fluctuations [94].

Many interesting PL and CL studies have been done as a function of temperature or pressure. With increasing pressure, the energy band gaps of nitrides increase, which can push some of the energy levels into the band gap to make them observable by optical measurements [95].

Frequently, experiments are performed as a function of temperature (from 4.2 to 300 K), from which an internal quantum efficiency η (IQE) can be extracted from the relation:

$$\eta = \frac{I(T)}{I(0)} \tag{1.3}$$

where $I(T)$ and $I(0)$ are the PL or CL intensities at a given temperature T and at 0 K, respectively.

At the same time, the IQE can be related to radiative non-radiative decay times:

$$\frac{1}{\eta} = 1 + \frac{\tau_r}{\tau_{\mathrm{nr}}} \tag{1.4}$$

Hence, from the experimental measurements of $I(0)$, $I(T)$, and τ, using Eqs. (1.2)–(1.4) makes possible to determine the quantum efficiency η and the radiative and the non-radiative decay times (τ_r and τ_{nr}).

However, the PL and CL data depend on excitation power and on the properties of the layers close to the active region. Hence, it is possible that the optimization of the optical active region (e.g. InGaN QWs) with respect to IQE is not reflected by higher efficiency of LEDs or LDs.

Figure 1.7 schematically depicts the typical layout of the most popular GaN-based optoelectronic devices, i.e. LEDs and LDs. In the case of LEDs, when the p–n junction is forward biased, the potential barrier of the junction is lowered and the recombination of electrons and holes can occur in the active region (e.g. a multiple quantum well, MQW), thus leading to photon emission. The challenge is not to have these photons absorbed or scattered in a wrong direction. For transparent sapphire substrates, it is possible to extract

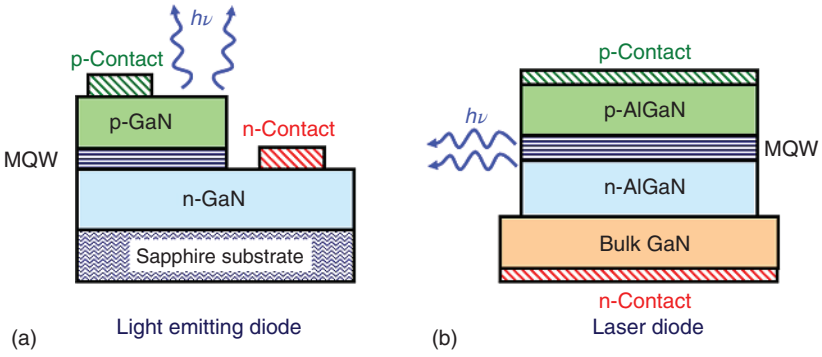

Figure 1.7 Simplified schemes of the two most popular GaN-based optoelectronic devices: (a) light-emitting diode (LED) and (b) edge emitting laser diode (LD). For LEDs, the light emission can be either through the back or upper surface. In the case of LDs, the light is confined between the cladding layers and is partially circulating between the mirrors on two edges of the chip.

light through them. For silicon substrates, the light extraction takes place only through the surface, which is not easy because of the presence of electrical contact. In the case of LDs, the light is confined between two AlGaN "cladding layers" and the light emission takes place through the edge covered with mirrors, which make photon circulate between two edges. For a low injection current, the light is emitted incoherently in a similar way to the LEDs. However, above a certain current threshold, a sufficiently high concentration of carriers is generated within the active region, leading to the population inversion. In this condition, electron–hole recombination is assisted by such photon and the stimulated emission takes place, dominating over the spontaneous one.

More details on LEDs and LDs operation principles and related technologies will be reported in Chapters 7–10.

1.2.3 Electrical Properties

GaN possess excellent electrical properties, which make it a promising material for electronic device fabrication.

First, the WBG of the material ($E_g = 3.4\,\text{eV}$) induces a high critical electric field ($E_{CR} = 3 - 3.75\,\text{MV/cm}$), which is the maximum field that the material can withstand without breakdown. As will be described in Section 1.3.2, the high critical field is a key factor for the realization of electronic devices operating at high voltages and with low on-resistance and high efficiency.

The temperature effects within the semiconductor must also be considered, as they have a strong influence on the carrier generation and, hence, on the electrical properties of the devices. In fact, the semiconductor device characteristics degrade by increasing the temperature, until their functionality for desired circuit applications is lost. Hence, an accurate control of the carrier (electrons and holes) concentration is needed. However, the dopant species are not the only source of carriers in a semiconductor. In fact, even in the absence of an intentional doping, every semiconductor would contain a certain amount of thermal carriers in

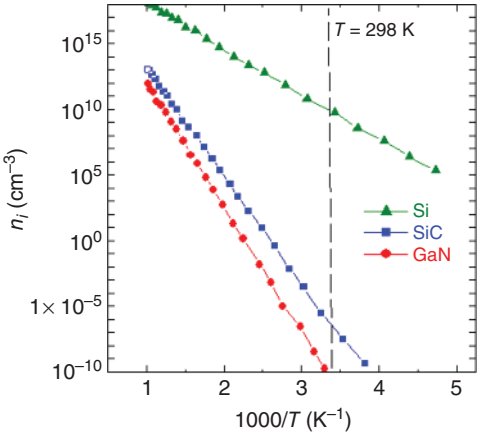

Figure 1.8 Calculated intrinsic carrier concentration n_i as a function of reverse of the temperature (1000/T) for GaN. For comparison, the curves of n_i for Si and SiC are also reported. The dashed line indicates the room temperature ($T = 298$ K). Source: Adapted from Neudeck et al. 2002 [96] and Baliga 2005 [97].

the crystal. The amount of these carriers is referred to as the intrinsic carrier concentration n_i, and it is exponentially dependent on temperature T:

$$n_i = \sqrt{N_C N_V} e^{-\frac{E_g}{2kT}} \tag{1.5}$$

where k is the Boltzmann constant and N_C and N_V are the density of the states in the conduction and valence bands, respectively.

Figure 1.8 reports the calculated intrinsic carrier concentration n_i of GaN as a function of the inverse of the temperature [96]. For comparison, the values of n_i for Si and SiC are also reported.

Noteworthy, if the temperature is increased, e.g. above 300 °C, in Si, the intrinsic carriers would become comparable or even higher than the intentional dopant concentration. Then, the electrical properties of the material would become undesirably influenced by the intrinsic carriers rather than by the designed doping needed for proper electrical operation [96]. From Figure 1.8, it is clear that SiC and GaN have much lower intrinsic carrier concentrations than Si. Hence, they do not suffer from intrinsic carrier conductivity issues even at a temperature of 600 °C. As an example, as can be seen in Figure 1.8, the intrinsic carrier concentration in GaN at room temperature ($T = 298$ K) is about 19 orders of magnitude lower than that of Si. Because of such a low value of n_i, the generation current is extremely low. Hence, GaN electronic devices should have theoretically a much lower leakage current with respect to Si and give the possibility to operate at higher temperatures.

However, it is important to point out that these considerations are valid for perfect crystals. In the reality, because of the large lattice mismatch between GaN and the substrate, the presence of material defects in GaN epitaxial layers, such as dislocations, typically provide preferential leakage pathways, which are a major obstacle for reaching the ideal electrical performances and low leakage in GaN electronic devices [98].

Figure 1.9 shows the calculated electron velocity of GaN as a function of the electric field [99]. As can be seen, the peak velocity in GaN is close to 3×10^7 cm/s and the saturation velocity is about 1.5×10^7 cm/s. These values are considerably higher than the values for GaAs and Si. Thanks to the high saturation velocity of

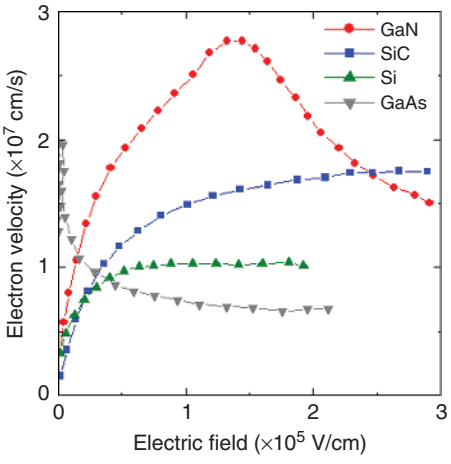

Figure 1.9 Electron velocity as a function of the electric field for GaN. For comparison, the values of the electron velocity of GaAs, Si, and SiC are also reported. Source: Adapted from Jain et al. 2000 [99] and Sze and Ng 2007 [100].

the carriers, it is possible to shorten the transit time in GaN electronic devices, thus allowing them to operate at high frequency, as will be better explained in Section 1.2.4.

Finally, the thermal conductivity of GaN is expected to vary in a certain range (1.3 – 2.1 W/cm K) depending on the defect density. These values are lower than those in SiC. Hence, SiC is better indicated for high-temperature applications than GaN. In fact, the heat dissipation in GaN devices must be appropriately managed, as will be discussed in Chapters 6 and 11.

Thanks to the properties mentioned above, significant advantages can be obtained using GaN-based devices, in terms of high-voltage, high-frequency, and high-temperature operation. To highlight these advantages, Figure 1.10 summarizes in a "radar chart" the electronic properties of GaN compared with those of Si and SiC. Here, it is worth mentioning that the reported material

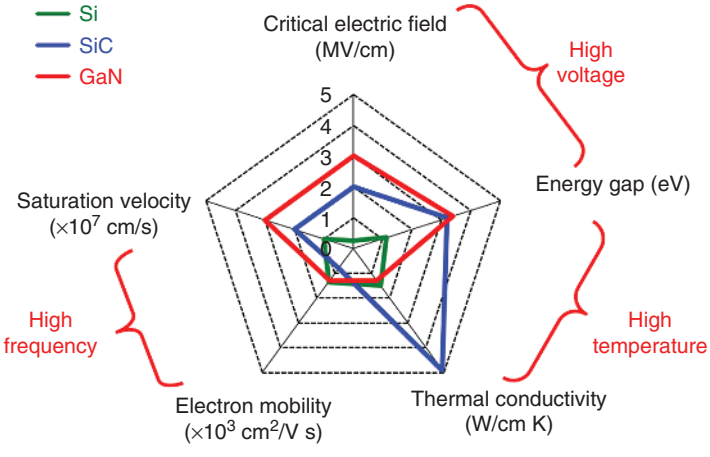

Figure 1.10 "Radar chart" of physical and electronic properties of GaN compared with those of Si and SiC.

properties may vary between different references. However, the graphic gives an idea of the great potential of this material.

1.2.4 Two-Dimensional Electron Gas (2DEG) in AlGaN/GaN Heterostructures

One of the most interesting features of nitride materials is the possibility to create alloys and heterostructures with tailored optical and electrical properties. An $Al_xGa_{1-x}N$ alloy is a hexagonal crystal that can be obtained by replacing in the GaN crystal a percentage of Ga-atoms with Al-atoms. As anticipated in Section 1.2.2, an important characteristic of the $Al_xGa_{1-x}N$ alloys is the possibility to tailor the lattice parameter and the energy gap by varying the Al concentration.

In particular, the in-plane lattice parameter a_0^{AlGaN} of the $Al_xGa_{1-x}N$ alloy and the Al-concentration x are correlated by the expression [19]:

$$a_0^{AlGaN}(x) = x a_0^{AlN} + (1-x) a_0^{GaN} \tag{1.6}$$

where a_0^{GaN} and a_0^{AlN} are the lattice parameters of GaN and AlN, respectively.

On the other hand, the energy gap $E_g^{AlGaN}(x)$ of an $Al_xGa_{1-x}N$ alloy can be written as a function of the energy gap of GaN E_g^{GaN} and AlN E_g^{AlN} [101]:

$$E_g^{AlGaN}(x) = x E_g^{AlN} + (1-x) E_g^{GaN} - x(1-x)1.0\ \text{eV} \tag{1.7}$$

where $b = 1.0$ eV is the bowing parameter typically used for AlGaN alloys [90].

The dependences of the in-plane lattice parameter a_0 and of the energy gap E_g on the Al-concentration x in an $Al_xGa_{1-x}N$ alloy are shown in Figure 1.11.

An *AlGaN/GaN heterostructure* can be formed by growing a thin $Al_xGa_{1-x}N$ barrier layer onto a GaN substrate along the [0001] crystallographic direction. Because of the different energy gaps of these two materials, an energy discontinuity will appear in the band diagram. Furthermore, the lattice mismatch between GaN and $Al_xGa_{1-x}N$ ($a_0^{GaN} > a_0^{AlGaN}$) will induce a tensile strain in

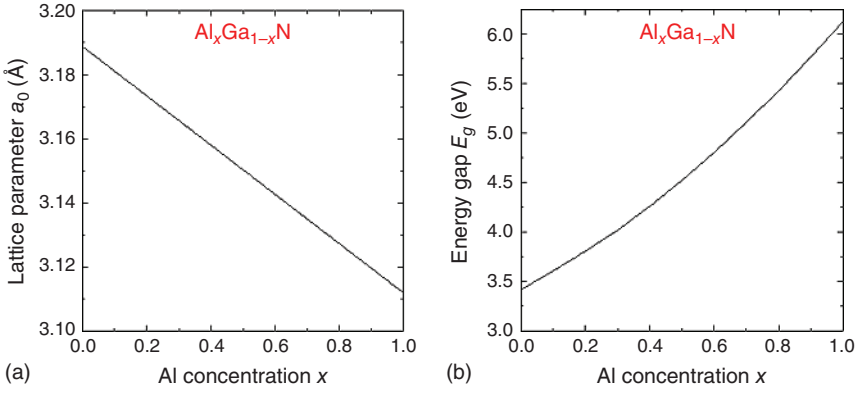

Figure 1.11 Dependence of the in-plane lattice parameter a_0 (a) and of the energy gap E_g (b) on the Al-concentration x in an $Al_xGa_{1-x}N$ alloy. Source: Adapted with permission of Roccaforte et al. [49]. Copyright © 2018, Società Italiana di Fisica.

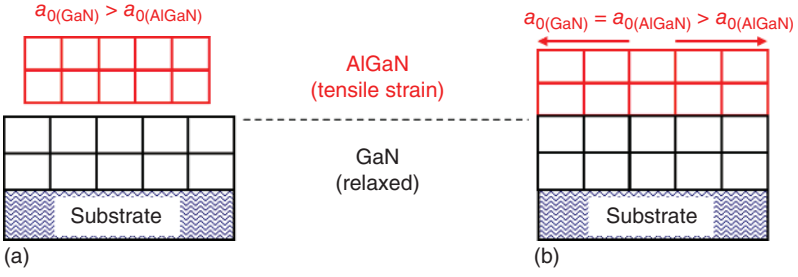

Figure 1.12 Schematic of isolated AlGaN and GaN crystals (a) and of the formed AlGaN/GaN heterostructure (b). After the growth of the AlGaN layer on GaN, a tensile strain is induced to compensate the lattice mismatch between the two materials. Source: Adapted with permission of Roccaforte et al. [49]. Copyright © 2018, Società Italiana di Fisica.

the $Al_xGa_{1-x}N$ *barrier layer* to compensate the in-plane lattice mismatch. This situation is schematically depicted in Figure 1.12, showing the isolated AlGaN and GaN crystals and the strained AlGaN/GaN heterostructure.

In the strained AlGaN/GaN heterostructure, a *piezoelectric polarization* $\boldsymbol{P}_{PE}$ will be induced along the *c*-axis, given by [19]:

$$P_{PE} = e_{33}\varepsilon_z + e_{31}(\varepsilon_x + \varepsilon_y) \tag{1.8}$$

where e_{33} and e_{31} are the piezoelectric coefficients, $\varepsilon_z = (c - c_0)/c_0$ is the strain along the *c*-axis, $\varepsilon_x = \varepsilon_y = (a - a_0)/a_0$ are the in-plane strains assumed to be isotropic, and a_0 and c_0 are the equilibrium lattice constants.

The piezoelectric polarization along the *c*-axis can be also expressed as [19]:

$$P_{PE} = 2\frac{a - a_0}{a_0}\left(e_{31} - e_{33}\frac{C_{13}}{C_{33}}\right) \tag{1.9}$$

where C_{13} and C_{33} are the elastic constants of the material.

Because the term $[e_{31} - e_{33}(C_{13}/C_{33})]$ is negative in the whole Al-concentration range typically used in $Al_xGa_{1-x}N$ alloys [19], the piezoelectric polarization will be negative for tensile strain ($a^{AlGaN} > a_0^{AlGaN}$) and positive for compressive strain ($a^{AlGaN} < a_0^{AlGaN}$). Hence, for a Ga-face AlGaN/GaN heterostructure with the AlGaN barrier layer under tensile strain, the piezoelectric polarization $\boldsymbol{P}_{PE}$ will be negative and parallel to the spontaneous polarization $\boldsymbol{P}_{SP}$ (directed toward the GaN substrate), as indicated in Figure 1.13a.

The polarization gradient existing at the AlGaN/GaN interface determines a polarization-induced charge density, which in turn depends on the Al-concentration *x*:

$$|\sigma(x)| = |[P_{SP}(Al_xGa_{1-x}N) + P_{PE}(Al_xGa_{1-x}N) - P_{SP}(GaN)]| \tag{1.10}$$

Hence, to maintain the charge neutrality in the system, free electrons will tend to compensate the polarization-induced charge density at the AlGaN/GaN interface, generating a *2DEG*. The 2DEG is accumulated in the potential well formed at the AlGaN/GaN interface (Figure 1.13b).

Ibbetson et al. [21] reported that the polarization-induced charges $\sigma(x)$ in Eq. (1.10) represent a dipole, whose net contribution to the total charge in the

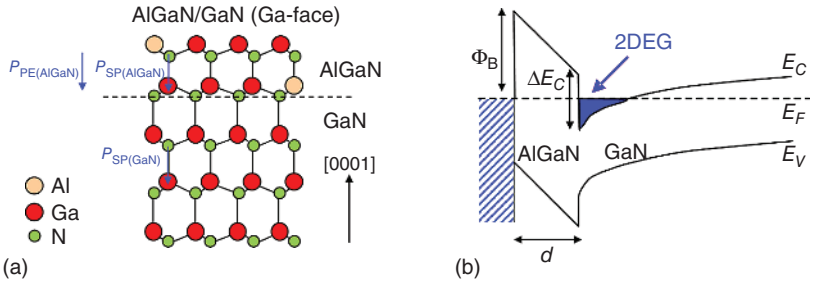

Figure 1.13 (a) Schematic of an AlGaN/GaN heterostructure, showing the spontaneous and piezoelectric polarization vectors and (b) schematic band diagram of an AlGaN/GaN heterostructure. The presence of 2DEG in the quantum well at the interface is indicated by the arrow. Source: Adapted with permission of Roccaforte et al. [49]. Copyright © 2018, Società Italiana di Fisica.

AlGaN/GaN system is zero. Accordingly, as no assumption can be made on the position of the Fermi level at the free surface of AlGaN, the presence of 2DEG can be explained by an electron transfer from donor-like surface states σ_{surface} placed at an energy E_D into empty states in GaN placed at a lower energy [21].

However, the situation occurring in a real device is different because the material surface is not free. In fact, in an AlGaN/GaN device, a Schottky metal electrode is formed on the AlGaN surface and the application of a bias is used to modulate the sheet carrier density of the 2DEG n_S. In the presence of a Schottky metal, the maximum sheet carrier density of the 2DEG can be expressed as [19]:

$$n_S(x) = \frac{\sigma(x)}{q} - \left[\frac{\varepsilon_0 \varepsilon_{\text{AlGaN}}(x)}{d_{\text{AlGaN}} q^2}\right] \cdot [q\Phi_B(x) + E_F(x) - \Delta E_C(x)] \tag{1.11}$$

where d_{AlGaN} is the $Al_xGa_{1-x}N$ barrier layer thickness, $\varepsilon_{\text{AlGaN}}$ is its permittivity, $q\Phi_B$ is the Schottky barrier height of the metal contact, E_F is the position of the Fermi level with respect to the GaN conduction band edge energy, and ΔE_C is the conduction band offset at the AlGaN/GaN interface.

Typically, the 2DEG generated in AlGaN/GaN heterostructures is characterized by sheet carrier density values in the order of 10^{13} cm^{-2} and mobility in the range of 1000–2000 cm^2/V s.

The *HEMT* is a device whose working principle is based on the presence of the 2DEG in AlGaN/GaN heterostructures. HEMT technology will be widely discussed in other chapters of this book.

A schematic cross section of this device is depicted in Figure 1.14a. In particular, in a conventional AlGaN/GaN HEMT, the current flowing in the 2DEG channel, between a source and a drain Ohmic electrode, is modulated by the application of a negative bias to a Schottky contact acting as a gate electrode of the transistor.

As the 2DEG is naturally present in the AlGaN/GaN heterostructure and the Fermi level at the interface lies above the conduction band minimum (see schematic in Figure 1.13b), such a device is "normally-on," i.e. a current will flow between source and drain even when the gate bias is zero ($V_g = 0$). An example of typical output I_{DS}–V_{DS} characteristic is depicted in Figure 1.14b. As can be

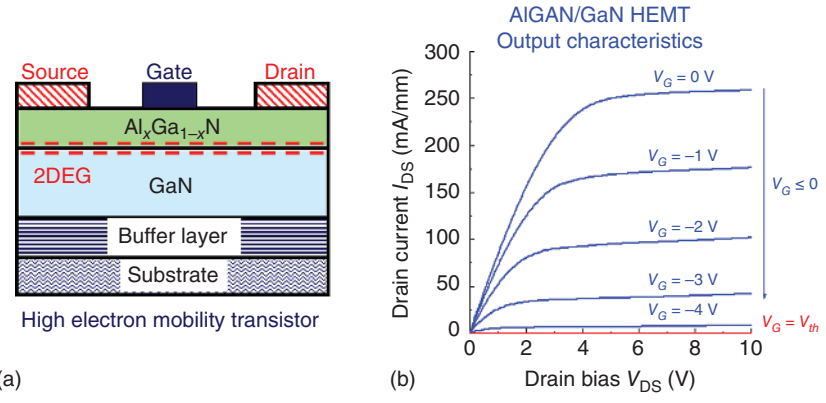

Figure 1.14 (a) Schematic cross section of an AlGaN/GaN HEMT and (b) typical output I_{DS}–V_{DS} characteristic of a device.

seen, the output current of a HEMT can be modulated by the application of a negative bias to the gate, until reaching a "threshold voltage" (V_{th}) when the Fermi level is pulled down below the conduction band edge of the AlGaN and the 2DEG channel is depleted.

The threshold voltage V_{th} of an AlGaN/GaN HEMT depends on the heterostructure properties (i.e. AlGaN thickness and doping, Al concentration) and can be written as [102]:

$$V_{th}(x) = \Phi_B(x) + E_F(x) - \Delta E_C(x) - \frac{qN_D d^2_{AlGaN}}{2\varepsilon_0 \varepsilon_{AlGaN}(x)} - \frac{\sigma(x)}{\varepsilon_0 \varepsilon_{AlGaN}(x)} d_{AlGaN} \tag{1.12}$$

where N_D is the doping density of the AlGaN barrier layer expressed in atoms/cm^3.

In normally-on HEMTs, the typical values of the AlGaN barrier thickness are of about 20–25 nm, with Al concentration in the range $x = 0.25$–0.30. In such AlGaN/GaN heterostructures, the values of the 2DEG sheet carrier density n_s are in the range of 0.7–1×10^{13} cm^{-2}, which results in negative values of V_{th} around −4 V. However, in power electronic applications, "normally-off" devices (i.e. with a $V_{th} > 0$) are strongly preferred [103–105]. A recent overview of the most common technologies for achieving normally-off HEMTs is given in Ref. [106]. This important topic will be discussed in Chapter 4.

The high saturation velocity of the material and the high mobility of the 2DEG in AlGaN/GaN heterostructures enable fast switching frequency of HEMTs. In fact, for high-frequency applications, it is necessary to shorten the transit time τ between the source–drain spacing L_{sd} of the switching transistor.

Considering the transit time of electron in the distance L_{sd}, the cutoff frequency f_T, i.e. the frequency at which the current gain becomes unity, can be written as:

$$f_T = \frac{1}{2\pi\tau} = \frac{v_{sat}}{2\pi L_{sd}} \tag{1.13}$$

which can be also expressed in terms of the transconductance g_m and of the gate capacitance C_g as:

$$f_T = \frac{g_m}{2\pi C_g} \tag{1.14}$$

Assuming the saturation electron velocity of GaN, from Eq. (1.13), it can be deduced that submicron gate HEMTs are able to operate at frequencies in the millimeter-wave (mmW) range [30].

The use of a Schottky contact as gate electrode in GaN-based HEMTs can be a limitation both for the off-state characteristics of the devices (i.e. leakage current) and for the maximum gate voltage swing (i.e. the current capability in the on-state). For that reason, the introduction of an insulating layer below the gate electrode is a common solution in GaN-based HEMT technology, especially for high-voltage applications. GaN HEMTs employing the insulated gate are often called *metal–insulator–semiconductor high-electron mobility transistors* (MISHEMTs). The problems related to insulated gate HEMTs will be discussed in the following chapters.

Some final considerations regard the heterostructures used for GaN-based HEMTs. Nowadays, GaN-based HEMTs for high-power and high-frequency operation are mostly fabricated using AlGaN/GaN heterostructures. However, the presence of a tensile stress in the AlGaN barrier layer, and the consequent relaxation effects, can be a limit of the heterostructure design. This aspect is particularly important for high-frequency applications, where a thinner barrier layer is needed to improve the capability of gate modulation, and to increase the device transconductance. Hence, a promising alternative to AlGaN as a barrier layer is the ternary alloy $In_xAl_{1-x}N$, which is lattice-matched to GaN for an InN mole fraction of around 17% [107]. At this composition, the stress and piezoelectric polarization are not present, thus potentially improving the stability of the heterostructure [108]. Even in the absence of piezoelectric polarization, the 2DEG sheet charge density induced by the difference in spontaneous polarization is typically larger than in the conventional AlGaN/GaN heterostructure. This should result in a higher output current and power density of the device [108]. Clearly, as discussed in Chapter 6, the high current densities achieved in InAlN/GaN HEMTs result in significant self-heating effects, which must be appropriately faced in order to limit detrimental effects for device reliability.

AlN/GaN heterostructures are another system that is particularly advantageous for high-frequency (mmW) HEMT operation. In fact, the use of an ultrathin (e.g. ~3 nm) AlN barrier ensures the submicrometric device scaling without incurring in the 2DEG degradation [109, 110]. Design considerations and critical processing steps for high-frequency AlN/GaN HEMTs will be discussed in Chapter 3.

1.3 Applications of GaN-Based Materials

GaN-based materials and heterostructures have several applications in both optoelectronic and power- and high-frequency devices. In the following sections,

a short overview of the main applications of nitride devices will be given, also mentioning some of the most relevant physical and technological open issues. These concepts will be useful as an introduction to the contents of the other chapters of the book devoted to devices.

1.3.1 Optoelectronic Devices

The scientific and technological achievements reached in nitride-based optoelectronic devices since the 1980s have led and are leading to creation of new multibillion markets. Figure 1.15 illustrates the examples of consumer applications of the nitride-based optoelectronic devices, i.e. LEDs and LDs, in several fields (general lighting, cars, video projections, etc.).

White LEDs have made a revolution in lighting, contributing significantly in a decrease of energy consumption. However, still white LEDs are not based on red–green–blue (RGB) emitters because green LEDs have too low efficiency (green gap). Instead, white LEDs are constructed using blue LEDs illuminating phosphor to excite light of longer wavelengths. Such white LEDs have become very popular, as they are used as bulbs or Christmas-tree illumination, but also in most of the computer screens.

Blue LEDs can be switched on and off much faster than the incandescent bulbs, thus making possible to use light to transmit information (Li-Fi instead of Wi-Fi). Even faster modulation (10 times compared to LEDs) can be achieved using blue LDs. Most likely, nitride-based LEDs and LDs will be widely used in smart cities to control traffic and other people activities in parallel to illumination.

Blue LDs are mostly recognized as those used in the BluRay for recording and playing the compact disks, although this technology will probably vanish soon. Nevertheless, nitride LDs have many other applications, e.g. they can be used for exciting phosphor to get white light. Such head lamps are produced and installed in luxury (so far) cars.

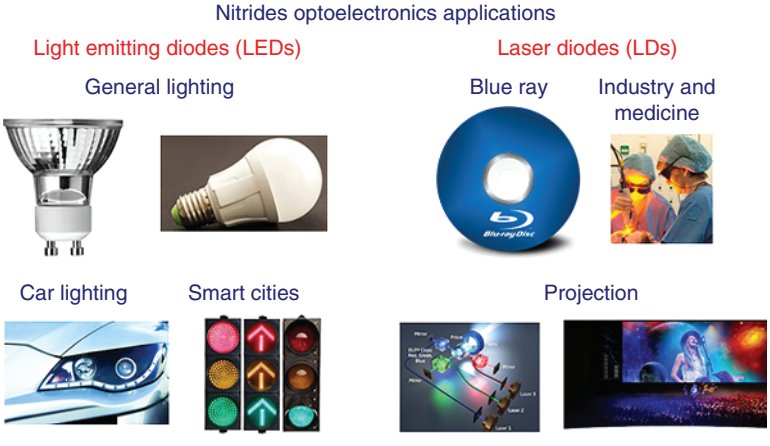

Figure 1.15 Examples of applications of nitrides devices (LEDs and LDs) in optoelectronics.

Lighting and Li-Fi are markets of tens-billion-Euro size, but even bigger one will be the one of RGB screens and movie projectors (blue and green emitters based on nitrides, red based on arsenides/phosphides). These RGB projectors will vary in size, the smallest for mobile phones, medium for TV sets, and the largest as billboards and for cinema theaters.

RGB screens based on LEDs are already installed as outdoor billboards. Each contains tens of thousands of LEDs. However, for the TV set and computer screens, not to mention the mobile phones, one needs much smaller pixels. This technology is almost ready, and RGB micro-LEDs will soon replace the other solutions.

Using RGB LDs makes it possible to obtain extra-high color resolution projectors, as well as to create three-dimensional images without using any goggles.

The third (after lighting and RGB projectors) huge market for GaN-based LDs could be "Last mile" Tb/s communication through plastic fibers. Such fibers can transmit 490 nm light and have a big advantage of being cheap, light, and more resistant to shocks as compared to glass waveguides. Therefore, they are of the first choice for battleships and army vehicles. Then, every house, aircraft, car, etc., could have such installation of plastic fibers to transmit data. However, it is not clear if the "Last mile" market will be developing because of the disadvantage of additional stage of signal processing.

A very interesting application of blue and green LDs of well-defined wavelengths is in the Quantum Technologies [111]. The LDs are used for cooling the atoms down to micro-kelvins and for exciting these atoms in atomic clocks, which are able to measure time with accuracy of fractions of picoseconds. Such clocks will enable GPS to measure the position with a high precision and to construct gravimeters to be used in geology and in detection of buried objects.

Moreover, there are several other niche markets for nitride LDs, e.g. in medicine, in environmental protection, as well as for welding of copper and gold.

Light in blue and green emitters is created in InGaN QWs, while using AlGaN enables to obtain UV radiation. Recent achievements of many laboratories in technology of 260–280 nm LEDs open interesting application perspectives in the disinfection of water, air, and food [112].

In the case of LDs, while the shortest wavelength demonstrated at the R&D level till 2019 has been of 340 nm [113], the commercially available devices operate in the range of 370–380 nm (www.nichia.co.jp/en/product/laser.html). Very recently, Z. Zhang et al. [38] demonstrated a deep UV device emitting at 271.8 nm in the pulse mode. The epitaxy of this device was done on bulk AlN crystal and p-doping was achieved by polarization-induced doping. The parameters (high voltage and high threshold current) of this deep UV LD were still far behind the devices emitting at the blue/green range, but this achievement will pave the way to the UV LDs, which would be used in medicine for sterilization or cancer curing via the waveguides.

In spite of the spectacular success of "GaNification" in optoelectronics, still there are many challenges that must be overcome.

The performance of blue and green LEDs is pegged back by three phenomena: droop (the gradual decrease in efficiency as the drive current increases), green gap (the gradual decrease in efficiency as the indium content in InGaN QWs

rises), and the electrical potential drop (increase in the voltage to be provided to increase current). An excellent discussion of those three phenomena is given by Han et al. [114].

On the other hand, in the case of nitride LDs, there are still many issues to be resolved. The low crystallographic quality, small size, and high price of GaN substrates is the main obstacle for a quick development of blue and green LD technology. As mentioned in Section 1.2.1, most of the nitride research- and-technology is based on foreign substrates, e.g. sapphire and silicon. The difference of lattice parameters and thermal expansion between GaN and those substrates results not only in a very high dislocation density but also in wafer bowing, which in turn makes lithography very difficult. The bulk GaN substrates are considered the future for optoelectronic devices, and in particular for LDs with long lifetime. Nowadays, such substrates are manufactured by number of companies all over the world (Sciocs, St. Gobain Lumilog, Furukawa, Nanowin, Ammono, Sumitomo, etc.). However, these crystals contain large densities of dislocations (10^4–10^7 cm^{-2}) and their size is typically limited to 2-inches, although 4- and 6-inches are already being introduced into the market. The prices of the GaN substrates are about 10 times higher than those of GaAs, or SiC, and even 100 times as compared to sapphire.

Another technical limitation is given by the low wall-plug efficiencies in the green region related to poor crystallographic quality and poor p-type of InGaN and GaN grown at low temperatures.

Finally, the lack of stimulated emission in the UV region related to poor p-type of AlGaN and the presence of point defects are also current bottlenecks in LD technology.

Many of these open issues will be discussed in Chapters 7–10.

1.3.2 Power- and High-Frequency Electronic Devices

Power electronics is the key enabling technology devoted to the control and management of electric power. In particular, the primary goal of a power electronic system is to provide the electric power in the optimal form (i.e. in terms of current, voltage, frequency, etc.) for the end user load. Hence, power electronic devices are used on a daily basis in our society in many fields, e.g. power supplies for computers, industrial motor drives, energy conversion systems in hybrid electric vehicles (HEVs), and inverters for renewable energies.

For some decades, silicon (Si) has been the semiconductor of choice for power devices because of its natural abundance, low cost, excellent crystalline quality, and device processing maturity. However, today, Si power devices have reached their operational limits, set by the intrinsic properties of the material, and are affected by significant power losses in practical applications. Hence, the improvement of energy efficiency in power electronics is one of the challenges of our society to reduce the global energy consumption. In this context, the introduction of new semiconductors technologies to overcome the current limitations of Si devices has become mandatory.

Because of their excellent electronic properties, WBG semiconductors are considered the materials of choice for the future energy efficient power devices [39].

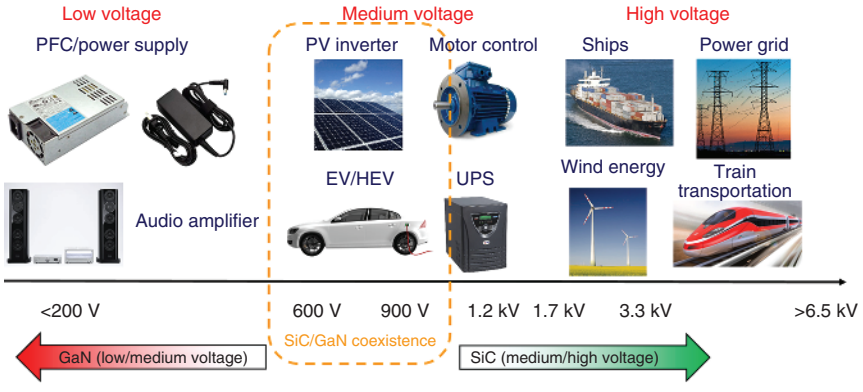

Figure 1.16 Potential applications of GaN power devices as a function of the voltage. For comparison, the application area of SiC is also indicated. Source: Adapted from Roccaforte et al. [106]. Copyright © 2019 by the authors; licensee MDPI, Basel, Switzerland. Reference [106] is an open access article distributed under the terms and conditions of the Creative Commons Attribution License.

Among them, while SiC [115] is the most fitted in terms of crystalline quality and device maturity, GaN and related alloys are very promising but still suffer from many concerns, which hinder their full exploitation in power electronic applications.

Figure 1.16 illustrates the potential applications of GaN devices in power electronics in the low-, medium-, and high-voltage range. For comparison, the typical range of application of the other WBG semiconductor SiC is also indicated.

According to the current opinion of market analysts, GaN could be better suited for the low-medium voltage range (200–600 V), which includes a part of the consumer electronic market (e.g. computer power supplies and audio amplifiers). In this voltage range, the material is the best candidate to replace the existing Si devices. The voltage range 600–900 V is strategic, as it covers the converters for electric vehicles (EVs) and HEV, and the inverters for renewable energy (e.g. photovoltaic). Here, GaN is expected to be in competition or to coexist with SiC. At higher voltage (>1.2 kV, e.g. industrial applications, trains/ships transportation, and electric energy distribution grids), 4H–SiC is considered as the preferable choice, owing to a better material quality and device reliability. The future applications of GaN for high-voltage devices will strongly depend on the improvement of the material quality and the development of vertical devices based on bulk GaN.

In general, considering the case of unipolar power devices, the specific on-resistance R_{ON} (expressed in $\Omega\,cm^2$) can be approximated by the contribution of the device drift layer [97]:

$$R_{ON} \cong \frac{4B_V^2}{\varepsilon_0 \varepsilon_{GaN} \mu_n E_{CR}^3} \tag{1.15}$$

where B_V is the targeted breakdown voltage, ε_{GaN} is the permittivity of GaN, μ_n is the electron mobility, and E_{CR} is the critical electric field of the material.

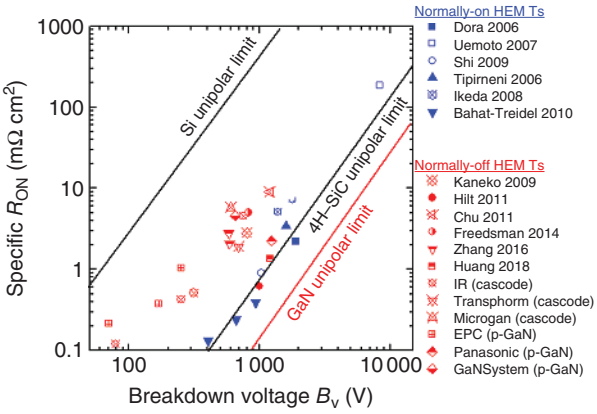

Figure 1.17 Trade-off of the specific on-resistance R_{ON} as a function of the breakdown voltage B_V for Si, 4H–SiC, and GaN. A collection of experimental literature data for normally-on and normally-off GaN HEMTs is also reported [45, 49, 116].

The high critical field E_{CR} of GaN enables the fabricated devices to sustain high-voltage levels with thinner drift layers. Hence, the specific on-resistance R_{ON} can be reduced and a smaller device area will be required to reach a given current. The low R_{ON} translates into a lower power dissipation in switching devices, which is a key requirement for a better energy efficiency in power electronic systems.

Figure 1.17 reports the theoretical trade-off between the specific on-resistance R_{ON} and the breakdown voltage B_V for Si, SiC, and GaN unipolar devices. A collection of literature data for GaN-based HEMTs (normally-on and normally-off) is also reported.

From this plot, it can be deduced that the theoretical limits are still far to be reached. The discrepancy between the state-of-the-art data and the theoretical limits can be associated with the existing issues in material quality and device processing [45, 49, 116, 117].

Metal/semiconductor contacts are important bricks of any electronic device. In particular, in GaN devices, the formation of Ohmic contacts with a low specific contact resistance ρ_c and Schottky contacts with an adequate barrier and a low leakage is required to minimize the device power consumption and improve the reliability [118].

The formation of Ohmic contacts with a low ρ_c is a challenging issue in GaN and related alloys. In fact, the values of metal/semiconductor Schottky barrier height on WBG semiconductors are typically higher than in Si and, hence, low values of ρ_c (in the order of 10^{-4}–$10^{-6}\ \Omega\,cm^2$) are difficult to obtain. Several metallization schemes have been proposed as Ohmic contacts to n-type GaN, as reported in a good review by Greco et al. [119].

In general, sequences of several metal layers are employed [120]. These stacks consist of a low work function metal (Ti) deposited on GaN and covered by an overlayer (Al). Then, a barrier layer is inserted to limit the interdiffusion between metals during annealing (Ni, Ti, Pt, Pd, Mo, etc.) and a top cap layer (Au) to prevent oxidation.

Recently, the interest toward GaN-based heterostructures grown on large-area Si substrates is grown because of the possibility of fabricating GaN devices using the Si CMOS facilities. In this context, to prevent contaminations and make GaN technology compatible with the Si CMOS line standards, the implementation of "Au-free" metallization schemes becomes mandatory.

On p-type GaN-based materials, the formation of Ohmic contacts is even more challenging because of the high metal/GaN barrier values and the high ionization energy of the Mg p-type dopant [121]. Also in the case of p-type GaN, various metal schemes have been investigated to form Ohmic contacts [119]. High work function metals (Ni, Pt, and Pd) are preferred, as they are expected to form a low Schottky barrier on the p-type semiconductor. Then, a cap layer of a noble metal (e.g. Au and Ag) is deposited on the top to prevent the oxidation. The Ni/Au bilayer is a very common scheme used for Ohmic contacts to p-GaN. Interestingly, Ohmic contact formation on p-type GaN is favored upon annealing in oxidizing atmosphere [122], with a complex mechanism that is widely debated in the literature.

The important role of contacts in GaN-based LEDs, LDs, and HEMTs will be mentioned in some chapters of the book.

Schottky contacts are used as gate metallization in GaN HEMTs to modulate the 2DEG concentration, Ni, Pt, and Au being the most widely used metals. However, the Schottky barriers on (Al)GaN often suffer from non-ideality issues and high leakage current, which limit the gate voltage swing in power transistors. Hence, dielectric materials can be used to insulate the Schottky gate and reduce the leakage current [123]. Moreover, dielectrics are very important as surface passivation to limit the so-called "current collapse" phenomena in GaN HEMTs [124–127] caused by the trapping of electrons at the device surface and/or in the buffer. Several dielectrics have been investigated as gate insulators and passivating layers for GaN HEMTs (SiN_x, SiO_2, Al_2O_3, etc.) [123, 128]. In this context, the reliability is an important concern in power electronic devices. As an example, a threshold voltage instability in GaN transistors can be detrimental in power switching applications. The occurrence of charge trapping effects at interfaces in the buffer layer or in the gate dielectrics are typically responsible for the V_{th} instability upon bias stress [129]. Typically, positive V_{th} shifts lead to a degradation of the device on-resistance, while negative V_{th} shifts can lead to the loss of the normally-off behavior. The reliability aspects associated with GaN electronic devices will be described in Chapter 6.

As described in Section 1.2.4, the HEMT working principle is based on the presence of the 2DEG conduction channel, making these devices inherently normally-on. Hence, the current is modulated by the application of a negative bias to a Schottky gate electrode. However, in power electronic applications, normally-off switches are preferred, as they provide fail-safe operation conditions and gate-driver circuitry simplicity [103–106]. Hence, the academic community and many industrial players working on GaN are spending significant efforts on the development of reliable normally-off technologies.

Under the physical point of view, to obtain the desired normally-off HEMT behavior, the region near the gate must be modified by employing appropriate near-surface processing or band engineering techniques. Several approaches

have been reported in the literature to achieve normally-off GaN-based HEMTs, the most common being the p-GaN gate and the recessed gate hybrid MISHEMT. The advantages and disadvantages of all these technologies will be critically described in Chapter 4.

In terms of operation frequency, the interest for the mmW band is steadily increasing, owing to the reduced wavelength and wide frequency bands, enabling smaller components with improved performances. In fact, today, the wireless communication systems are extending to higher frequencies because of the need for more bandwidth for several emerging applications. In this context, GaN-based devices can represent the best choice for high-power amplifiers (HPAs), broadband amplifiers, and 5G wireless communication networks. However, also in this case, several technological challenges need to be overcome in order to achieve the optimal device performance, as will be discussed in Chapter 3.

Clearly, the high-frequency performances of GaN-based HEMTs are ultimately limited by the lateral scaling of the device channel. In this context, the integration of two-dimensional (2D) materials with nitrides has recently opened the way toward alternative devices beyond the HEMTs, targeted for ultra-high-frequency operation. As an example, the hot electron transistor (HET) is a device based on the transversal ballistic transport of hot electrons through an ultrathin base layer. As will be discussed in the Chapter 11, graphene junctions with Al(Ga)N/GaN heterostructures have been recently employed to implement vertical HETs potentially able to work in the terahertz frequency range.

Finally, it is worth mentioning that GaN electronics is dominated by lateral transistors fabricated on AlGaN/GaN heterostructures grown on foreign substrates. However, vertical devices based on bulk GaN are strongly desired in power electronics. In fact, the vertical topology can enable to increase the breakdown voltage by increasing the thickness of the drift region, while maintaining the chip size constant. Furthermore, the maximum electric field in vertical GaN devices is moved far away from the surface into the bulk, thus enabling to minimize the trapping phenomena and to eliminate the current collapse. Not least, vertical devices on high-quality bulk GaN crystals can allow to achieve a higher power density than lateral devices, thanks to the lower R_{ON} and higher current capability and to the higher thermal conductivity of the bulk material. The status and perspectives of vertical GaN devices will be discussed in Chapter 5.

1.4 Summary

In summary, this chapter gave an overview of the main physical, optical, and electrical properties of GaN-based materials. The direct band gap, combined with the possibility to have the desired wavelength by tailoring the composition, is the key aspect that allowed use of nitride semiconductors in optoelectronics successfully. However, the outstanding characteristics, in terms of electric field

strength and piezoelectric properties of AlGaN/GaN heterostructures, also make these semiconductors excellent candidates for the next generation of power- and high-frequency devices.

Although GaN-based devices (LEDs, LDs, and transistors) have already entered our daily life, there are still many problems related to material growth and device processing that deserve further intensive research.

Acknowledgments

The authors would like to thank their coworkers and the coauthors of the other book chapters for the fruitful inputs provided during the preparation of this chapter. This work is the outcome of a long-standing collaboration between the Institute for Microelectronics and Microsystems of the National Research Council of Italy (CNR-IMM) in Catania and the Institute of High Pressure Physics of the Polish Academy of Sciences (Unipress-PAS) in Warsaw. In particular, the authors would like to acknowledge the bilateral project ETNA (*Energy efficiency Through Novel AlGaN/GaN heterostructures*) within the CNR-PAS Cooperation Agreement for the years 2017–2019 and the bilateral project GaNIMEDE (*Gallium Nitride Innovative Micro-Electronics DEvices*) within the Executive Programme for Scientific and Technological Cooperation between The Italian Republic and the Republic of Poland for the years 2019–2020.

References

1 Johnson, W.C., Parsons, J.B., and Crew, M.C. (1932). Nitrogen compounds of gallium – III. gallium nitride. *J. Phys. Chem.* 36: 2651–2654.
2 Juza, R. and Hahn, H. (1938). Über die Kristallstrukturen von Cu_3N, GaN und InN metallamide und metallnitride. *Z. Anorg. Allg. Chem.* 239: 282–287.
3 Maruska, H.P. and Tietjen, J.J. (1969). The preparation and properties of vapor-deposited single-crystalline GaN. *Appl. Phys. Lett.* 15: 327–329.
4 Maruska, H.P., Stevenson, D.A., and Pankove, J.I. (1973). Violet luminescence of Mg-doped GaN. *Appl. Phys. Lett.* 22: 303–305.
5 Manasevit, H.M., Erdmann, F.M., and Simpson, W.I. (1971). The use of metalorganics in the preparation of semiconductor materials – IV. The nitrides of aluminum and gallium. *J. Electrochem. Soc.* 118: 1864–1868.
6 Manasevit, H.M. (1972). The use of metalorganics in the preparation of semiconductor materials: growth on insulating substrates. *J. Cryst. Growth* 13–14: 306–314.
7 Karpinski, J., Jun, J., and Porowski, S. (1984). Equilibrium pressure of N_2 over GaN and high-pressure solution growth of GaN. *J. Cryst. Growth* 66: 1–10.
8 Karpinski, J. and Porowski, S. (1984). High-pressure thermodynamics of GaN. *J. Cryst. Growth* 66: 11–20.

9 Amano, H., Sawaki, N., Akasaki, I., and Toyoda, Y. (1986). Metalorganic vapor phase epitaxial growth of a high quality GaN film using an AlN buffer layer. *Appl. Phys. Lett.* 48: 353–355.

10 Amano, H., Kito, M., Hiramatsu, K., and Akasaki, I. (1989). P-type conduction in Mg-doped GaN treated with low-energy electron beam irradiation (LEEBI). *Jpn. J. Appl. Phys.* 28: L2112–L2114.

11 Matsuoka, T., Tanaka, H., Sasaki, T., and Katsui, A. (1990). Gallium arsenide and related comp. *Inst. Phys. Conf. Ser.* 106: 141.

12 Nakamura, S., Senoh, M., and Mukai, T. (1991). High-power GaN P–N junction blue-light-emitting diodes. *Jpn. J. Appl. Phys.* 30, 1991: L1708–L1711.

13 Nakamura, S., Mukai, T., Senoh, M., and Iwasa, N. (1992). Thermal annealing effects on P-type Mg-doped GaN films. *Jpn. J. Appl. Phys.* 31: L139–L142.

14 Asif Khan, M., Van Hove, J.M., Kuznia, J.N., and Olson, D.T. (1991). High electron mobility GaN/$Al_xGa_{1-x}N$ heterostructures grown by low-pressure metalorganic chemical vapor deposition. *Appl. Phys. Lett.* 58: 2408–2410.

15 Aisf Khan, M., Bhattarai, A.R., Kuznia, J.N., and Olson, D.T. (1993). High electron mobility transistor based on a GaN/$Al_xGa_{1-x}N$ heterojunction. *Appl. Phys. Lett.* 63: 1214–1215.

16 Nakamura, S., Senoh, M., Nagahama, S. et al. (1996). InGaN-based multi-quantum-well-structure laser diodes. *Jpn. J. Appl. Phys.* 35: L74–L76.

17 Bernardini, F., Fiorentini, V., and Vanderbilt, D. (1997). Spontaneous polarization and piezoelectric constants of III–V nitrides. *Phys. Rev. B* 56: R10024–R10027.

18 Guha, S. and Bojarczuk, N.A. (1998). Ultraviolet and violet GaN light emitting diodes on silicon. *Appl. Phys. Lett.* 72: 415–417.

19 Ambacher, O., Smart, J., Shealy, J. et al. (1999). Two-dimensional electron gases induced by spontaneous and piezoelectric polarization charges in N- and Ga-face AlGaN/GaN heterostructures. *J. Appl. Phys.* 85: 3222–3233.

20 Sheppard, S.T., Doverspike, K., Pribble, W.L. et al. (1999). High-power microwave GaN/AlGaN HEMT's on semi-insulating silicon carbide substrates. *IEEE Electron Device Lett.* 20: 161–163.

21 Ibbetson, J.P., Fini, P.T., Ness, K.D. et al. (2000). Polarization effects, surface states, and the source of electrons in AlGaN/GaN heterostructure field effect transistors. *Appl. Phys. Lett.* 77: 250–252.

22 Motoki, K., Okahisa, T., Matsumoto, N. et al. (2001). Preparation of large freestanding GaN substrates by hydride vapor phase epitaxy using GaAs as a starting substrate. *Jpn. J. Appl. Phys.* 40: L140–L143.

23 Motoki, K. (2010). Development of gallium nitride substrates. *SEI Tech. Rev.* 70: 28–35.

24 Saito, W., Takada, Y., Kuraguchi, M. et al. (2006). Recessed-gate structure approach toward normally-off high-voltage AlGaN/GaN HEMT for power electronics applications. *IEEE Electron Device Lett.* 53: 356–362.

25 Cai, Y., Zhou, Y., Lau, K.M., and Chen, K.J. (2006). Control of threshold voltage of AlGaN/GaN HEMTs by fluoride-based plasma treatment: from depletion mode to enhancement mode. *IEEE Electron Device Lett.* 53: 2207–2215.

26 Uemoto, Y., Hikita, M., Ueno, H. et al. (2007). Gate injection transistor (GIT) – a normally-off AlGaN/GaN power transistor using conductivity modulation. *IEEE Trans. Electron Devices* 54: 3393–3399.

27 Lu, T.-C., Kao, C.-C., Kuo, H.-C. et al. (2008). CW lasing of current injection blue GaN-based vertical cavity surface emitting laser. *Appl. Phys. Lett.* 92 (2008): 141102.

28 Tripathy, S., Lin, V.K.X., Tan, J.P.Y. et al. (2012). AlGaN/GaN two-dimensional-electron gas heterostructures on 200 mm diameter Si(111). *Appl. Phys. Lett.* 101: 082110.

29 Iveland, J., Martinelli, L., Peretti, J. et al. (2013). Direct measurement of Auger electrons emitted from a semiconductor light-emitting diode under electrical injection: identification of the dominant mechanism for efficiency droop. *Phys. Rev. Lett.* 110: 177406.

30 Shinohara, K., Regan, D.C., Tang, Y. et al. (2013). Scaling of GaN HEMTs and Schottky diodes for submillimeter-wave MMIC applications. *IEEE Trans. Electron Devices* 60 (10): 2982–2996.

31 Freedsman, J.J., Egawa, T., Yamaoka, Y. et al. (2014). Normally-OFF Al_2O_3/AlGaN/GaN MOS-HEMT on 8 in. Si with low leakage current and high breakdown voltage (825 V). *Appl. Phys. Express* 7: 041003.

32 Kikkawa, T., Hosoda, T., Shono, K. et al. (2015). Commercialization and reliability of 600 V GaN power switches. Proceedings of IEEE International Reliability Physics Symposium (IRPS 2015), Monterey, CA (19–23 April 2015), 6C.1.1.

33 Kaneko, S., Kuroda, M., Yanagihara, M. et al. (2015). Current-collapse-free operations up to 850 V by GaN-GIT utilizing hole injection from drain. Proceedings of the 27th International Symposium on Power Semiconductor Devices & IC's (ISPSD2015), Kowloon Shangri-La, Hong Kong (10–14 May 2015), pp. 41–44.

34 Tanaka, K., Morita, T., Umeda, H. et al. (2015). Suppression of current collapse by hole injection from drain in a normally-off GaN-based hybrid-drain-embedded gate injection transistor. *Appl. Phys. Lett.* 107 (16): 163502.

35 Tanaka, K., Morita, T., Ishida, M. et al. (2017). Reliability of hybrid-drain-embedded gate injection transistor. Proceedings of IEEE International Reliability Physics Symposium (IRPS 2017), Monterey, CA (2–6 April 2017), 4B-2.1.

36 Haller, C., Carlin, J.-F., Jacopin, G. et al. (2017). Burying non-radiative defects in InGaN underlayer to increase InGaN/GaN quantum well efficiency. *Appl. Phys. Lett.* 111: 262101.

37 Mei, Y., Weng, G.-E., Zhang, B.-P. et al. (2017). Quantum dot vertical-cavity surface-emitting lasers covering the 'green gap'. *Light Sci. Appl.* 6: e16199. https://doi.org/10.1038/lsa.2016.199.

38 Zhang, Z., Kushimoto, M., Sakai, T. et al. (2019). A 271.8 nm deep ultraviolet laser diode for room temperature operation. *Appl. Phys. Express* 12 (12): 124003.

39 Ren, F. and Zolper, J.C. (2003). *Wide Band Gap Electronic Devices*. Singapore: World Scientific.

40 Pearton, S.J., Abernathy, C.R., and Ren, F. (2006). *Gallium Nitride Processing for Electronics, Sensors and Spintronics*. Springer Verlag-London Ltd.

41 Quai, R. (2008). *Gallium Nitride Electronics*. Berlin Heidelberg: Springer-Verlag.

42 Meneghini, M., Meneghesso, G., and Zanoni, E. (2017). *Power GaN Devices – Materials, Applications and Reliability*. Switzerland: Springer International Publishing.

43 Roccaforte, F., Giannazzo, F., Iucolano, F. et al. (2010). Surface and interface issues in wide band gap semiconductor electronics. *Appl. Surf. Sci.* 256: 5727–5735.

44 Kizilyalli, I.C., Edwards, A.P., Nie, H. et al. (2013). High voltage vertical GaN p–n diodes with avalanche capability. *IEEE Trans. Electron Devices* 60: 3067–3070.

45 Roccaforte, F., Fiorenza, P., Greco, G. et al. (2014). Challenges for energy efficient wide band gap semiconductor power devices. *Phys. Status Solidi (a)* 211: 2063–2071.

46 Grabowski, S.P., Schneider, M., Nienhaus, H. et al. (2001). Electron affinity of $Al_xGa_{1-x}N$ (0001) surfaces. *Appl. Phys. Lett.* 78: 2503–2505.

47 Cook, T.E., Fulton, C.C., Mecouch, W.J. et al. (2003). Band offset measurements of the Si_3N_4/GaN (0001) interface. *J. Appl. Phys.* 94: 3949–3953.

48 Caldas, P.G., Silva, E.M., Prioli, R. et al. (2017). Plasticity and optical properties of GaN under highly localized nanoindentation stress fields. *J. Appl. Phys.* 121: 125105.

49 Roccaforte, F., Fiorenza, P., Lo Nigro, R. et al. (2018). Physics and technology of gallium nitride materials for power electronics. *Riv. Nuovo Cimento* 41: 625–681.

50 Leszczyński, M., Teisseyre, H., Suski, T. et al. (1996). Lattice parameters of gallium nitride. *Appl. Phys. Lett.* 69: 73–75.

51 Darakchieva, V., Monemar, B., and Usui, A. (2007). On the lattice parameters of GaN. *Appl. Phys. Lett.* 91: 031911.

52 Arehart, A., Homan, T., Wong, M.H. et al. (2010). Impact of N- and Ga-face polarity on the incorporation of deep levels in n-type GaN grown by molecular beam epitaxy. *Appl. Phys. Lett.* 96: 242112.

53 Yu, E.T., Dang, X.Z., Asbeck, P.M. et al. (1999). Spontaneous and piezoelectric polarization effects in III–V nitride heterostructures. *J. Vac. Sci. Technol. B* 17: 1742–1749.

54 Taniyasu, Y., Kasu, M., and Kobayashi, N. (2001). Lattice parameters of wurtzite $Al_xSi_{1-x}N$ ternary alloys. *Appl. Phys. Lett.* 79: 4351–4353.

55 Nilsson, D., Janzén, E., and Kakanakova-Georgieva, A. (2016). Lattice parameters of AlN bulk, homoepitaxial and heteroepitaxial material. *J. Phys. D. Appl. Phys.* 49: 175108.

56 Paszkowicz, W., Adamczyk, J., Krukowski, S. et al. (1999). Lattice parameters, density and thermal expansion of InN microcrystals grown by the reaction of nitrogen plasma with liquid indium. *Philos. Mag. A* 79: 1145–1154.

57 Kröncke, H., Figge, S., Epelbaum, B.M., and Hommel, D. (2008). Determination of the temperature dependent thermal expansion coefficients of bulk AlN by HRXRD. *Acta Phys. Pol. A* 114: 1193–1200.

58 Leszczyński, M., Suski, T., Teisseyre, H. et al. (1994). Thermal expansion of gallium nitride. *J. Appl. Phys.* 76: 4909–4911.

59 Liu, L. and Edgar, J.H. (2002). Substrates for gallium nitride epitaxy. *Mater. Sci. Eng. R* 37: 61–127.

60 Krost, A. and Dadgar, A. (2002). GaN-based optoelectronics on silicon substrates. *Mater. Sci. Eng. B* 93: 77–84.

61 Kizilyalli, I.C., Bui-Quanga, P., Disney, D. et al. (2015). Reliability studies of vertical GaN devices based on bulk GaN substrates. *Microelectron. Reliab.* 55: 1654–1661.

62 Zhang, N.Q., Moran, B., DenBaars, S.P., Mishra, U.K., Wang, X.W., Ma, T.P. (2001). Effects of surface traps on breakdown voltage and switching speed of GaN power switching HEMTs. Technical Digest – International Electron Devices Meeting, 2001 (IEDM '01), Washington, DC (2–5 December 2001) pp. 589–592.

63 Lee, C.D., Sagar, A., Feenstra, R.M. et al. (2001). Growth of GaN on SiC(0001) by molecular beam epitaxy. *Phys. Status Solidi (a)* 188: 595–599.

64 Choi, S., Heller, E., Dorsey, D. et al. (2013). Analysis of the residual stress distribution in AlGaN/GaN high electron mobility transistor. *J. Appl. Phys.* 113: 093510.

65 Böttcher, T., Einfeldt, S., Figge, S. et al. (2001). The role of high-temperature island coalescence in the development of stresses in GaN films. *Appl. Phys. Lett.* 78: 1976–1978.

66 Ishida, M., Ueda, T., Tanaka, T., and Ueda, D. (2013). GaN on Si technologies for power switching devices. *IEEE Trans. Electron Devices* 60: 3053–3059.

67 Chen, K.J., Häberlen, O., Lidow, A. et al. (2017). GaN-on-Si power technology: devices and applications. *IEEE Trans. Electron Devices* 64: 779–795.

68 Leszczyński, M., Prystawko, P., Suski, T. et al. (1999). Lattice parameters of GaN single crystals, homoepitaxial layers and heteroepitaxial layers on sapphire. *J. Alloys Compd.* 286: 271–275.

69 Prystawko, P., Leszczyński, M., Beaumont, B. et al. (1998). Doping of homoepitaxial GaN layers. *Phys. Status Solidi B* 210: 437–443.

70 Sarzynski, M., Leszczyńki, M., Krysko, M. et al. (2012). Influence of GaN substrate off-cut on properties of InGaN and AlGaN layers. *Cryst. Res. Technol.* 47: 321–328.

71 Suski, T., Staszczak, G., Grzanka, S. et al. (2010). Hole carrier concentration and photoluminescence in magnesium doped InGaN and GaN grown on sapphire and GaN misoriented substrates. *J. Appl. Phys.* 108: 023516.

72 Sarzyński, M., Suski, T., Staszczak, G. et al. (2012). Lateral control of indium content and wavelength of III–nitride diode lasers by means of GaN substrate patterning. *Appl. Phys. Express* 5: 021001.

73 Krysko, M., Domagala, J.Z., Czernecki, R., and Leszczyński, M. (2013). Triclinic deformation of InGaN layers grown on vicinal surface of GaN (00.1) substrates. *J. Appl. Phys.* 114: 113512.

74 Zauner, A., Aret, E., Enckevort, W. et al. (2002). Homo-epitaxial growth on the N-face of GaN single crystals: the influence of the misorientation on the surface morphology. *J. Cryst. Growth* 240: 14–21.

75 Smeeton, T., Kappers, M., Barnard, J. et al. (2003). Electron-beam-induced strain within InGaN quantum wells: false indium "cluster" detection in the transmission electron microscope. *Appl. Phys. Lett.* 83: 5419–5421.

76 Baloch, K.H., Johnston-Peck, A.C., Kisslinger, K. et al. (2013). Revisiting the "In-clustering" question in InGaN through the use of aberration-corrected electron microscopy below the knock-on threshold. *Appl. Phys. Lett.* 102: 191910.

77 Michałowski, P., Grzanka, E., Grzanka, S. et al. (2019). Indium concentration fluctuations in InGaN/GaN quantum wells. *J. Anal. At. Spectrom.* 34: 1718–1723.

78 Suihkonen, S., Svensk, O., Lang, T. et al. (2007). The effect of InGaN/GaN MQw hydrogen treatment and threading dislocation optimization on GaN LED efficiency. *J. Cryst. Growth* 298: 740–743.

79 Czernecki, R., Grzanka, E., Smalc-Koziorowska, J. et al. (2015). Effect of hydrogen during growth of quantum barriers on the properties of InGaN quantum wells. *J. Cryst. Growth* 414: 38–41.

80 Czernecki, R., Grzanka, E., Strak, P. et al. (2017). Influence of hydrogen pre-growth flow on indium incorporation into InGaN layers. *J. Cryst. Growth* 464: 123–126.

81 Hestroffer, K., Wu, F., Li, H. et al. (2015). Relaxed c-plane InGaN layers for the growth of strain-reduced InGaN quantum wells. *Semicond. Sci. Technol.* 30: 105015.

82 Sarzynski, M., Krysko, M., Targowski, G. et al. (2006). Elimination of AlGaN epilayer cracking by spatially patterned AlN mask. *Appl. Phys. Lett.* 88: 121124.

83 Cicek, E., McClintock, R., Vashaei, Z. et al. (2013). Crack-free AlGaN for solar-blind focal plane arrays through reduced area epitaxy. *Appl. Phys. Lett.* 102: 051102.

84 Arslan, E., Ozturk, M.K., Teke, A. et al. (2008). Buffer optimization for crack-free GaN epitaxial layers grown on Si(111)substrate by MOCVD. *J. Phys. D. Appl. Phys.* 41: 155317.

85 Schubert, E.F. (2006). *Light-Emitting Diodes*, 2e. New York: Cambridge University Press.

86 Orsal, G., El Gmili, Y., Fressengeas, N. et al. (2014). Bandgap energy bowing parameter of strained and relaxed InGaN layers. *Opt. Mater. Express* 4: 1030–1041.

87 Gu, G.-H., Jang, D.-H., Nam, K.-B., and Park, C.-G. (2013). Composition fluctuation of In and well-width fluctuation in InGaN/GaN multiple quantum wells in light-emitting diode devices. *Microsc. Microanal.* 19 (S5): 99–104.

88 Ochalski, T.J., Gil, B., Bigenwald, P. et al. (2001). Dual contribution to the stokes shift in InGaN–GaN quantum wells. *Phys. Status Solidi B* 228 (1): 111–114.

89 Moses, P.G. and Van de Walle, C.G. (2010). Band bowing and band alignment in InGaN alloys. *Appl. Phys. Lett.* 96: 021908.

90 Yun, F., Reschikov, M.A., He, L. et al. (2002). Energy band bowing parameter in $Al_xGa_{1-x}N$ alloys. *J. Appl. Phys.* 92 (8): 4837–4839.

91 Kazazis, S.A., Papadomanolaki, E., Androulidaki, M. et al. (2018). Optical properties of InGaN thin films in the entire composition range. *J. Appl. Phys.* 123: 125101.

92 Paskov, P.P. and Monemar, B. (2018). Optical properties of III-nitride semiconductors. *Handbook of GaN Semiconductor Materials and Devices*. Bi, W.W., Kuo, H-C., Ku, P-C., Shen, B. Edts. CRC Press/Taylor & Francis Group, Boca Raton, FL, pag. 83.

93 Reschikov, M.A. and Morkoç, H. (2005). Luminescence properties of defects in GaN. *J. Appl. Phys.* 97: 061301.

94 Wang, Y.J., Xu, S.J., Zhao, D.G. et al. (2006). Non-exponential photoluminescence decay dynamics of localized carriers in disordered InGaN/GaN quantum wells: the role of localization length. *Opt. Express* 14 (26): 13151–13157.

95 Perlin, P., Suski, T., Teisseyre, H. et al. (1995). Towards the identification of the dominant donor in GaN. *Phys. Rev. Lett.* 75: 296–299.

96 Neudeck, P.G., Okojie, R.S., and Chen, L.-Y. (2002). High temperature electronics – a role for wide bandgap semiconductors? *Proc. IEEE* 90: 1065–1076.

97 Baliga, B.J. (2005). *Silicon Carbide Power Devices*. Singapore: World Scientific Publishing.

98 Arehart, R., Moran, B., Speck, J.S. et al. (2006). Effect of threading dislocation density on Ni/n-GaN Schottky diode I–V characteristics. *J. Appl. Phys.* 100: 023709.

99 Jain, S.C., Willander, M., Narayan, J., and Van Overstraeten, R. (2000). III-nitrides: growth, characterization and properties. *Appl. Phys. Rev.* 87: 965–1006.

100 Sze, M.S. and Ng, K.K. (2007). *Physics of Semiconductor Devices*, 3e. Hoboken, NJ: Wiley.

101 Brunner, D., Angerer, H., Bustarret, E. et al. (1997). Optical constants of epitaxial AlGaN films and their temperature dependence. *J. Appl. Phys.* 82: 5090–5096.

102 Asgari, A. and Kalafi, M. (2006). The control of two-dimensional-electron-gas density and mobility in AlGaN/GaN heterostructures with Schottky gate. *Mater. Sci. Eng. C* 26: 898–901.

103 Chen, K.J. and Zhou, C. (2011). Enhancement-mode AlGaN/GaN HEMT and MIS-HEMT technology. *Phys. Status Solidi (a)* 208: 434–438.

104 Su, M., Chen, C., and Rajan, S. (2013). Prospects for the application of GaN power devices in hybrid electric vehicle drive systems. *Semicond. Sci. Technol.* 28: 074012.

105 Scott, M.J., Fu, L., Zhang, X. et al. (2013). Merits of gallium nitride based power conversion. *Semicond. Sci. Technol.* 28: 074013.

106 Roccaforte, F., Greco, G., Fiorenza, P., and Iucolano, F. (2019). An overview of normally-off GaN-based high electron mobility transistors. *Materials* 12: 1599.

107 Carlin, J.-F. and Ilegems, M. (2003). High-quality AlInN for high index contrast Bragg mirrors lattice matched to GaN. *Appl. Phys. Lett.* 83: 668–670.

108 Medjdoub, F., Carlin, J.F., Gaquière, C. et al. (2008). Status of the emerging InAlN/GaN power HEMT technology. *The Open Electr. Electron. Eng. J.* 2: 1–7.

109 Medjdoub, F., Zegaoui, M., Waldhoff, N. et al. (2011). Above 600 mS/mm transconductance with 2.3 A/mm drain current density AlN/GaN high-electron-mobility transistors grown on silicon. *Appl. Phys. Express* 4: 064106.

110 Harrouche, K., Kabouche, R., Okada, E., and Medjdoub, F. (2019). High performance and highly robust AlN/GaN HEMTs for millimeter-wave operation. *IEEE J. Electron Devices Soc.* 7: 1145–1150.

111 Najda, S.P., Perlin, P., Suski, T. et al. (2017). AlGaInN diode-laser technology for optical clocks and atom interferometry. *J. Phys. Conf. Ser.* 810: 012052.

112 Nyangaresi, P.O., Qin, Y., Chen, G. et al. (2018). Effects of single and combined UV-LEDs on inactivation and subsequent reactivation of *E. coli* in water disinfection. *Water Res.* 147: 331–341.

113 Yamashita, Y., Kuwabara, M., Torii, K., and Yoshida, H. (2013). A 340-nm-band ultraviolet laser diode composed of GaN well layers. *Opt. Express* 21 (3): 3133–3137.

114 Han, D.P., Kamiyama, S., Takeuchi, T. et al. (2019). Understanding inefficiencies in blue and green LEDs. *Compd. Semicond.* 25 (3): 56–61.

115 Kimoto, T. and Cooper, J.A. (2014). *Fundamentals of Silicon Carbide Technology: Growth, Characterization, Devices and Applications*. Singapore: Wiley.

116 Amano, H., Baines, Y., Borga, M. et al. (2018). The 2018 GaN power electronics roadmap. *J. Phys. D. Appl. Phys.* 51: 163001.

117 Roccaforte, F., Fiorenza, P., Greco, G. et al. (2018). Emerging trends in wide band gap semiconductors (SiC and GaN) technology for power devices. *Microelectron. Eng.* 187–188: 66–77.

118 Chung, J.W., Roberts, J.C., Piner, E.L., and Palacios, T. (2008). Effect of gate leakage in the subthreshold characteristics of AlGaN/GaN HEMTs. *IEEE Electron Device Lett.* 29: 1196–1198.

119 Greco, G., Iucolano, F., and Roccaforte, F. (2016). Ohmic contacts to gallium nitride materials. *Appl. Surf. Sci.* 383: 324–345.

120 Mohammad, S.N. (2004). Contact mechanisms and design principles for alloyed Ohmic contacts to n-GaN. *J. Appl. Phys.* 95: 7940–7953.

121 Roccaforte, F., Frazzetto, A., Greco, G. et al. (2012). Critical issues for interfaces to p-type SiC and GaN in power devices. *Appl. Surf. Sci.* 258: 8324–8333.

122 Greco, G., Prystawko, P., Leszczyński, M. et al. (2011). Electro-structural evolution and Schottky barrier height in annealed Au/Ni contacts onto p-GaN. *J. Appl. Phys.* 110: 123703.

123 Roccaforte, F., Fiorenza, P., Greco, G. et al. (2014). Recent advances on dielectrics technology for SiC and GaN power devices. *Appl. Surf. Sci.* 301: 9–18.
124 Daumiller, I., Theron, D., Gaquière, C. et al. (2001). Current instabilities in GaN-based devices. *IEEE Electron Device Lett.* 22: 62–64.
125 Binari, S.C., Ikossi, K., Roussos, J.A. et al. (2001). Trapping effects and microwave power performance in AlGaN/GaN HEMTs. *IEEE Trans. Electron Devices* 48: 465–471.
126 Vetury, R., Zhang, N.Q., Keller, S., and Mishra, U.K. (2001). The impact of surface states on the DC and RF characteristics of AlGaN/GaN HFETs. *IEEE Trans. Electron Devices* 48: 560–566.
127 Meneghesso, G., Verzellesi, G., Pierobon, R. et al. (2004). Surface-related drain current dispersion effects in AlGaN-GaN HEMTs. *IEEE Trans. Electron Devices* 51: 1554–1561.
128 Hashizume, T., Nishiguchi, K., Kanekia, S. et al. (2018). State of the art on gate insulation and surface passivation for GaN-based power HEMTs. *Mater. Sci. Semicond. Process.* 78: 85–95.
129 Meneghesso, G., Meneghini, M., De Santi, C. et al. (2018). Positive and negative threshold voltage instabilities in GaN-based transistors. *Microelectron. Reliab.* 80: 257–265.